2009-09

Aerodynamic performance predictions of a SA-2 Missile using Missile Datcom

Maurice, Andrew F.

Monterey, California. Naval Postgraduate School

NAVAL POSTGRADUATE SCHOOL

MONTEREY, CALIFORNIA

THESIS

AERODYNAMIC PERFORMANCE PREDICTIONS OF A SA-2 MISSILE USING MISSILE DATCOM

by

Andrew F. Maurice

September 2009

Thesis Advisor:	Muguru Chandrasekhara
Second Reader:	Christopher Brophy

Approved for public release; distribution is unlimited

THIS PAGE INTENTIONALLY LEFT BLANK

REPORT DOCUMENTATION PAGE		Form Approved OMB No. 0704-0188

1. AGENCY USE ONLY *(Leave blank)*	2. REPORT DATE September 2009	3. REPORT TYPE AND DATES COVERED Master's Thesis

4. TITLE AND SUBTITLE Aerodynamic Performance Predictions of a SA-2 Missile using Missile DATCOM	5. FUNDING NUMBERS
6. AUTHOR(S) Andrew F. Maurice	
7. PERFORMING ORGANIZATION NAME(S) AND ADDRESS(ES) Naval Postgraduate School Monterey, CA 93943-5000	8. PERFORMING ORGANIZATION REPORT NUMBER
9. SPONSORING /MONITORING AGENCY NAME(S) AND ADDRESS(ES) MSIC/DIA, Huntsville, AL	10. SPONSORING/MONITORING AGENCY REPORT NUMBER

11. SUPPLEMENTARY NOTES The views expressed in this thesis are those of the author and do not reflect the official policy or position of the Department of Defense or the U.S. Government.

12a. DISTRIBUTION / AVAILABILITY STATEMENT Approved for public release; distribution is unlimited	12b. DISTRIBUTION CODE

13. ABSTRACT (maximum 200 words)

This study reports an analysis of the aerodynamic performance characteristics of an SA-2 type missile conducted using empirical codes. The Missile and Space Intelligence Center (MSIC) supplied the missile geometry, which was incorporated into the MissileLab interface. The study evolved based on the geometry changes MSIC recommended. Results obtained using Missile DATCOM versions 7/07 and 8/08 are compared along with performance data provided by the project sponsor. These data varied from experimental to empirical, as well as those generated using Simulink modeling. Data comparisons were carried out for various Mach numbers and angles of attack. For the most part, excellent agreement was obtained, especially when Missile DATCOM 8/08 was used, for the overall axial force coefficient value at the conditions explored validating the approach used. Some comparisons also were generated for specific fin deflections conditions. Additionally, a Computational Fluid Dynamics model was included as part of the analysis, using ANSYS CFX, a compressible flow solver. With these results and the predictive tool, the in-house capability at the Naval Postgraduate School to generate such data for future missile designs has been successfully enhanced.

14. SUBJECT TERMS Missile Aerodynamics, Missile DATCOM, Missilelab, SA-2 Missile	15. NUMBER OF PAGES 77
	16. PRICE CODE

17. SECURITY CLASSIFICATION OF REPORT	18. SECURITY CLASSIFICATION OF THIS PAGE	19. SECURITY CLASSIFICATION OF ABSTRACT	20. LIMITATION OF ABSTRACT
Unclassified	Unclassified	Unclassified	UU

NSN 7540-01-280-5500 Standard Form 298 (Rev. 2-89)
Prescribed by ANSI Std. 239-18

THIS PAGE INTENTIONALLY LEFT BLANK

Approved for public release; distribution is unlimited

AERODYNAMIC PERFORMANCE PREDICTIONS OF A SA-2 MISSILE USING MISSILE DATCOM

Andrew F. Maurice
Lieutenant, United States Navy
B.S., University of Florida, 2001

Submitted in partial fulfillment of the
requirements for the degree of

MASTER OF SCIENCE IN MECHANICAL ENGINEERING

from the

NAVAL POSTGRADUATE SCHOOL
September 2009

Author: Andrew F. Maurice

Approved by: Muguru Chandrasekhara
Thesis Advisor

Christopher Brophy
Second Reader

Knox Millsaps
Chairman, Department of Mechanical and Astronautical Engineering

THIS PAGE INTENTIONALLY LEFT BLANK

ABSTRACT

This study reports an analysis of the aerodynamic performance characteristics of an SA-2 type missile conducted using empirical codes. The Missile and Space Intelligence Center (MSIC) supplied the missile geometry, which was incorporated into the MissileLab interface. The study evolved based on the geometry changes MSIC recommended. Results obtained using Missile DATCOM versions 7/07 and 8/08 are compared along with performance data provided by the project sponsor. These data varied from experimental to empirical, as well as those generated using Simulink modeling. Data comparisons were carried out for various Mach numbers and angles of attack. For the most part, excellent agreement was obtained, especially when Missile DATCOM 8/08 was used, for the overall axial force coefficient value at the conditions explored validating the approach used. Some comparisons also were generated for specific fin deflections conditions. Additionally, a Computational Fluid Dynamics model was included as part of the analysis, using ANSYS CFX, a compressible flow solver. With these results and the predictive tool, the in-house capability at the Naval Postgraduate School to generate such data for future missile designs has been successfully enhanced.

THIS PAGE INTENTIONALLY LEFT BLANK

TABLE OF CONTENTS

LIST OF FIGURES

LIST OF TABLES

THIS PAGE INTENTIONALLY LEFT BLANK

ACKNOWLEDGMENTS

Many thanks go to Professor Chandrasekhara, without whom this endeavor would not be possible. His guidance and patience have strengthened my will to complete this study.

I owe my family a debt of gratitude. Without their unwavering devotion, I would not have the strength to carry on this task.

Lastly, I would like to thank my classmates for their support and constant encouragement during this process.

THIS PAGE INTENTIONALLY LEFT BLANK

NOMENCLATURE

AFRL	Air Force Research Lab
AFB	Air Force Base
AGARD	Advisory Group for Aerospace Research and Development
AIAA	American Institute of Aeronautics and Astronautics
AMRDEC	Aviation and Missile Research, Development, and Engineering Center
AOA	Angle of Attack
CFD	Computational Fluid Dynamics
EOM	Equations of Motion
MAE	Mechanical and Astronautical Engineering
MDAC	McDonnell Douglas Aircraft Company
MSIC	Missile and Space Intelligence Center
NACA	National Advisory Committee for Aeronautics
NASA	National Air and Space Agency
NEAR	Nielsen Engineering and Research, Inc.
NSWC	Naval Surface Warfare Center
SOSE	Second Order Shock Expansion
USAF	United States Air Force
VDHT	Van Dyke Hybrid Theory
C_D	Drag Coefficient (wind axis)
C_L	Lift Coefficient (wind axis)
C_A	Axial Force Coefficient (body axis)
C_N	Normal Force Coefficient (body axis)
C_p	Pressure Coefficient
$C_{A,0}$	Axial Force Coefficient at Zero Angle of Attack
$C_{A,\alpha}$	Axial Force Coefficient Due to Angle of Attack
C_{Apres}	Axial Force Coefficient Due to Pressure Drag
$C_{Apres\text{-}trun}$	Axial Force Coefficient Due to Pressure Drag for a Truncated Nose Geometry

C_{Aform}	Axial Force Coefficient Due to Form Drag
C_{Afric}	Axial Force Coefficient Due to Skin Friction
C_f	Skin Friction Coefficient Invariant of Angle of Attack
$C_{A,\delta}$	Axial Force Coefficient Due to Control Surface Deflection Angle
M	Mach Number
V	Velocity
m	Mass
T	Thrust
α	Angle of Attack
q	Dynamic Pressure
S	Reference Area
g	Gravitational Acceleration
χ	Flight Path Angle
h	Altitude
Φ	Total Aerodynamic Potential
r	Radial Coordinate Variable
φ	Angular Coordinate Variable
x	Axial Coordinate Variable
M_∞	Freestream Mach Number
β	$\sqrt{1-M^2}$
r_b	Body Radius
ψ	Axial Flow Potential Solution
ζ	Cross Flow Potential Solution
ξ	Dummy Variable of Itegration
γ	Ratio of Specific Heats
U_∞	Freestream Velocity
u	X-direction Perturbation Velocity (Cartesian Coordinate System)
v	Y-direction Perturbation Velocity (Cartesian Coordinate System)
w	Z-direction Perturbation Velocity (Cartesian Coordinate System)
k	Induced Drag Parameter

I. INTRODUCTION

A. RESEARCH MOTIVATION

During conceptual and preliminary missile design, having a timely and good estimate of the aerodynamic performance of the design is valuable. By having this information early, the designer is able to estimate range, size the propulsion system, and determine how maneuverable the finished product can be. This information can then be used to ensure that customer requirements are adhered to from early on in the project. From a reverse engineering standpoint, use of this type of information enables the determination of the capabilities of a missile design gained through intelligence efforts. Further, such an analysis provides the necessary design requirements for building a missile defense system to counter the threat. The ability to produce such computer predictions without the actual expense of building either a scaled or an actual model is clearly invaluable.

Aerodynamic prediction software packages provide a design tool to quickly generate aerodynamic performance estimates. Distinct from Computational Fluid Dynamics (CFD), these software packages primarily use semi-empirical methods for this purpose, as opposed to discretizing the flow field and solving the Navier-Stokes equations at each point. Some of these prediction packages are Missile DATCOM, Aerodynamic Prediction Code (AP-XX), PANEL3D, PRODAS V3, SET3D, and NEAR MISL3.

The advantage of quick estimates for the performance of a flight vehicle is generally accepted even though the related uncertainty is about ±10%. The United States Air Force's Missile DATCOM software package, originally created by McDonnell Douglas Aircraft Company, was the tool employed for the current study. It was used to determine the flight characteristics, specifically axial force, of the Russian-designed SA-2 missile. Experimental and extrapolated data for this configuration was available from the sponsor (MSIC, Missile and Space Intelligence Center). Through careful comparison between the wind tunnel/extrapolated data and that produced by Missile DATCOM,

validation of the Missile DATCOM product became possible, thus furthering its use as a predictive tool in conceptual and preliminary design efforts.

B. TACTICAL MISSILE DRAG ESTIMATION

1. General Concepts

In aerodynamic design of an aircraft or missile, lift and drag are its two major and critical characteristics. A framework is needed to discuss how these forces act on the body. In Eqs. (1)–(3), a representation of the EOM from Krieger et al. (Mendenhall & Hemsch, 1992, p. 3) for a point-mass trajectory (in-plane, flat-Earth [curvature effects not included]), the dependence of the velocity and flight angle on the lift and drag coefficients is evident.

$$\frac{dV}{dt} = \frac{1}{m}\left(T\cos\alpha - C_D qS\right) - g\sin\chi \tag{1}$$

$$\frac{d\chi}{dt} = \frac{\left(T\sin\alpha + C_L qS\right)}{mV} - \frac{g\cos\chi}{V} \tag{2}$$

$$\frac{dh}{dt} = V\sin\chi \tag{3}$$

For missile aerodynamics, it is customary to work in body axis coefficients, the axial force and normal force coefficients, C_A and C_N. Eqs. (4) and (5) show the relationship between the body coordinate representation of the forces and the traditional representations of lift and drag.

$$C_D = C_A\cos\alpha + C_N\sin\alpha \tag{4}$$

$$C_L = C_N\cos\alpha - C_A\sin\alpha \tag{5}$$

From Eqs. (1)–(3), one can see that for every time step in a numerical solution to produce the velocity, flight path angle, and change in altitude, the quantities of lift and

drag must be known. To this end, the aerodynamicist must produce a large and accurate database of aerodynamic coefficients for a range of flight conditions to accurately represent a missile's behavior. The aerodynamic prediction software packages provide this capability.

Aerodynamic lift is important to maintain the missile in flight. However, drag is of greater interest because it governs the ability of the missile to achieve the speeds necessary to intercept and neutralize a threat. It is also more complex to calculate. Therefore, only drag prediction methods are discussed in this chapter.

2. Component Build-up Method

Conventional missiles consist of a circular cylindrical body with distinct wings and tails and are typically axisymmetric. For these types of missiles, the primary method for computing drag is the component build-up method (Mendenhall & Hemsch, 1992). This approach consists of identifying the individual distinct features of the missile such as the wings, tails and inlets, and calculating the drag produced by each of these separately. Figure 1 gives a graphic representation of the process to use the component build-up method. The influence of the individual parts on other features is often relatively small and, thus, is neglected. All of the individual drag components are summed to get the final total for the whole body, hence the name "component build-up." For a non-conventional missile (i.e., a blended body design), the interference between individual parts is often not small and thus cannot be neglected. In this case, the component build-up method does not produce very accurate results.

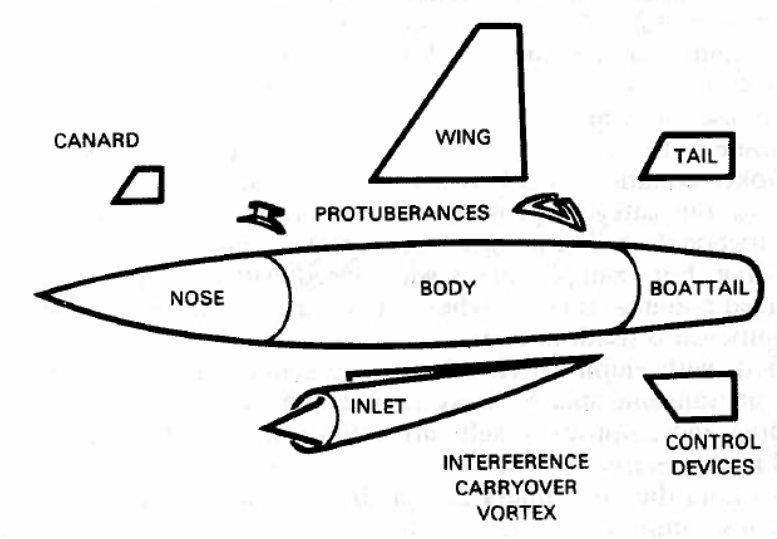

Figure 1. Component Build-up model (From Mendenhall & Hemsch, 1992, p. 7)

a. Body Drag

Body drag is separated into the drag that is produced in the boundary layer due to skin friction and the drag produced due to pressure distribution over the body (forebody pressure drag and base drag). The assumption of the separation of drag components breaks down at subsonic speeds and high angles of attack. Most tactical missiles spend a very short time in the subsonic region. However, because of the inherent nature of missile flight operations (radical maneuvers, etc.) high angle of attack flight is of considerable interest.

It is well known (Mendenhall & Hemsch, 1992) that more than 50% of the drag at zero angle of attack is due to the missile body. In the subsonic region, the axial force is dominated by skin friction. However, during the transition from the transonic region to the supersonic region, contribution of skin friction to the total axial force decreases and wave drag becomes dominant. Krieger and Vukelich (Mendenhall & Hemsch, 1992) state that for most components of the missile body, the drag predictions are theoretically based. However, transonic afterbodies and base drag do not lend themselves to this type of calculation. Empirical methods with experimental foundations are often necessary.

Figure 2 shows the typical variation of drag at zero angle of attack while changing the freestream Mach number. Clearly, in the subsonic region through the beginning of the transonic region, the drag coefficient is relatively constant. As the Mach number increases through M = 1.0, a large increase in the drag coefficient is noticed. This is caused by the onset of shock waves and the continued strengthening of these shocks, which increases the wave drag significantly. In later discussions of the experimental data for the SA-2, this transonic drag rise will be clearly seen.

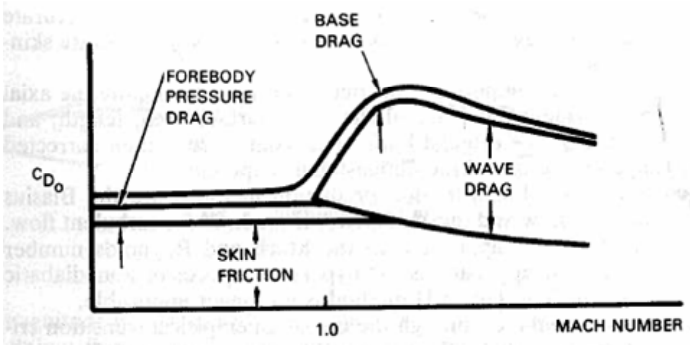

Figure 2. Drag component variation with Mach number (From Mendenhall & Hemsch, 1992, p. 8)

Typical formulations for skin friction involve computing the axial force equivalent for a flat plate and then correcting it with a 3D shape factor. An equivalent flat plate is one that has the same surface area, length, and Reynolds number as the body. Because of this formulation, laminar and turbulent boundary layer states must be taken into account. The axial force for laminar boundary layers is calculated using the Blasius formulation. The axial force resulting from turbulent boundary layers is typically calculated using the Van Driest method. These are combined in regards to transition from laminar flow to turbulent flow via an empirical transition criterion (Mendenhall & Hemsch, 1992).

Forebody pressure drag must be discussed in relation to the flight speed region in which the body is operating. In the subsonic region, the pressure drag increases as the Reynolds number increases along the body due to the thickening of the boundary layer and eventual flow separation. In the transonic region, the production of shockwaves on the body plays an integral role. Slender body theory and the transonic

area rule are methods for calculating forebody drag in this region. When the flight regime becomes fully supersonic, local shocks no longer appear on the body and bow and stern shocks attach to the body. Because of the attached shocks at the nose, wave drag dominates. Van Dyke's hybrid theory (VDHT) and second-order shock expansion (SOSE) theory are typically used to calculate the forces.

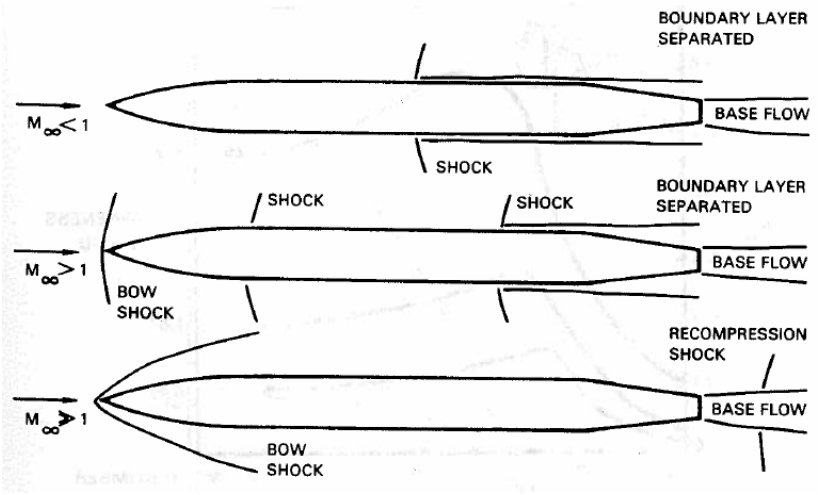

Figure 3. Missile body flow changes with increasing Mach number (From Mendenhall & Hemsch, 1992, p. 11)

Figure 3 gives a graphical representation of the changes that occur on the typical missile body as the freestream Mach number is increased. One thing to note is that shock interactions with the body can cause the flow to separate, thus increasing the drag considerably, especially in the transonic region. Base flow is also depicted here, which results in base drag, another component of pressure drag on the body. A base pressure that is lower than the freestream induces the base drag. The dead air in the base region is entrained in the external flow and carried downstream by mixing processes in the shear layers of the flow. Krieger and Vukelich describe this process as "scavenging," which reduces the pressure in the base region below the freestream, thus producing the base drag (Mendenhall & Hemsch, 1992).

b. Inlet Drag and Fin Drag

Inlet drag is typically comprised of the drag that is produced as part of a thrust-making effort (e.g., jet engine, ramjet) It usually is separated into boundary layer

diverter drag, ram drag (for bleed air), additive wave drag, cowl wave drag, internal skin friction (i.e., head loss), inlet fairing drag, and inlet fairing base drag. This list, although not complete, describes most physical phenomena that are occurring (Mendenhall & Hemsch, 1992).

Fin drag is computed in a manner similar to the body drag. It is broken into skin friction and pressure drag. Skin friction calculation methods use the flat plate assumption, but the correlation is much closer when compared to body drag, so a correction may not be used depending on the required accuracies for the prediction. The pressure drag is slightly more complicated to compute, but the same flow features manifest themselves on the fins in the transition from subsonic to supersonic conditions as occur on the body. Figure 4 shows a graphical representation of this transition with three Mach number regimes.

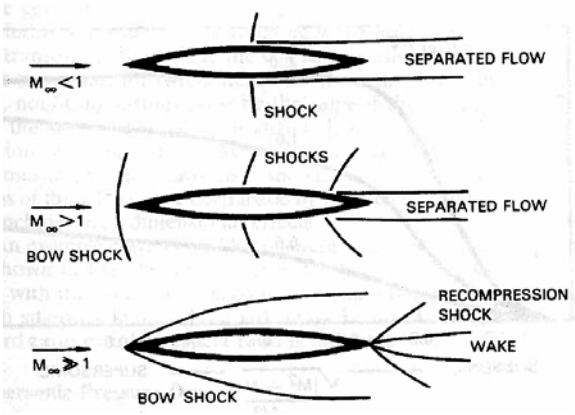

Figure 4. Missile fin flow changes with increasing Mach number (From Mendenhall & Hemsch, 1992, p. 21)

In the subsonic region, the pressure drag correlates with the thickness-to-chord (t/c) ratio and skin friction. As the fin enters the transonic region, shocklets begin to form, which are normal to the surface. As the speed increases, a bow shock forms and attaches to the body, and the normal shocks no longer appear on the surface. Recompression shocks can be seen attached to the trailing edge at the wake. In the transonic region, the transonic area rule and von Kármán similarity laws are used to

calculate the wave drag. In the supersonic region, linear supersonic theory, Busemann Theory, and shock expansion theory are used to calculate the wave drag if the bow shock is attached.

C. AERODYNAMIC PREDICTION SOFTWARE EMPLOYED

Missile DATCOM-08 was used in the present study. It is an aerodynamic prediction software package that has been updated to incorporate the newer coding features of FORTRAN 90 and is maintained by the US Army Aviation and Missile Research, Development, and Engineering Center (AMRDEC) in conjunction with the Air Vehicles Directorate of the Air Force Research Laboratory (AFRL), Wright Patterson AFB, Ohio. Missile DATCOM's allure as a useful tool in the preliminary design of a wide variety of missiles stems from the speed at which it is able to produce useful and accurate predictions of a missile's aerodynamic characteristics. Both the current and previous versions of the software (7/07 and 8/08) are used as part of this study. Tables 5–7 of Appendix B summarize the methods for calculating axial force coefficient for the body and fins and their combined effect in the body-fin synthesis.

D. SUPERSONIC AERODYNAMIC PREDICTION THEORIES

The SA-2 is primarily a supersonic missile. Thus, a discussion of the supersonic prediction theories is relevant. Missile DATCOM uses the VDHT and SOSE theory to calculate missile flight parameters in the supersonic region. Since the Mach number of interest here was 0.8 and higher, no discussion of the subsonic methods employed by Missile DATCOM will be made. Hypersonic Newtonian Theory (HNT) is additionally used in the high supersonic to hypersonic regimes and where SOSE theory is possibly valid as well, but experimental data is not available for the missile configuration being studied, so a discussion of HNT is also not included.

Van Dyke's hybrid theory combines a second-order axial solution to the full potential equation with a first order cross flow solution. Perturbations in the flow resulting from the presence of the body affect the axial direction more prominently than the cross flow direction. The second order solution is thus required in the axial direction to obtain the desired accuracy. Since the presence of the body has a smaller effect in the

cross flow direction, only a first-order solution is required to obtain the desired accuracy. These two solutions are then combined linearly to form a solution to the full potential equation. Subsequently, the perturbation velocities arise from this solution and enable the calculation of the pressure coefficient. The pressure coefficient is then integrated over the body to get the axial and normal force coefficients. A more detailed explanation including equations is presented in Appendix A for VDHT.

Syvertson and Dennis (1957) developed SOSE theory in the late 1950s from the first-order shock expansion theory first proposed by Eggers et al. (1953). In first-order theory, the flow parameters are computed at the leading edge of a two-dimensional surface with oblique shock wave relations or with a conical solution for a three-dimensional body. Prandtl-Meyer expansion calculations are then performed along the surface at different points to determine the pressure distribution over the body. For curved bodies, at each point, conical tangent elements are used and the pressure is assumed to be constant over each individual element. In order to get an accurate pressure distribution, a sufficient number of points must be used to approximate the curvature of the body. Syvertson and Dennis proposed that a second-order solution be employed because, the first order calculations were not accurate for axial force computations. The main difference between first and second order is that in second order, the pressure is not assumed to be constant over each conical tangent element but varies in a roughly exponential fashion (Moore, 2000).

E. SURVEY OF RECENT IMPROVEMENTS TO MISSILE DATCOM

Table 1 chronicles the recent version history of Missile DATCOM from 2002 to the present revision. The most important capabilities and changes that are applicable to this research manifest in release 9 and release 11.

Release	Revision	Capabilities Added or Changes Made
8	09/02	High AOA, airfoil, friction drag corrections
9	01/06	Code clean-up and restructuring Cambered body capability Revised body drag (bluntness, high AOA)
10	07/07	Rolling moment for elliptical bodies Improvements in TE flap control increments Improvements for low aspect ratio fins
11	08/08	Ability to have nine fin sets with 8 fins each Revised body drag Moment contribution for protuberances

Table 1. Recent Version History for Missile DATCOM (After Auman, Doyle, Rosema, Underwood, & Blake, 2008)

Horton and McDaniel (2005) performed a study in 2005 to determine the inaccuracies in the 09/02 version of Missile DATCOM with the intention of incorporating the proposed changes into the 01/06 version. Their study had particular emphasis on axial force calculations. In the 09/02 version, subsonic axial force for $0 < \alpha < 30^{\circ}$ is calculated by considering a part of the force that is invariant with angle of attack and a part that changes with angle of attack as shown in Eq. (6). This methodology was suggested by Allen and Perkins (1951).

$$C_A = C_{A,0} + C_{A,\alpha} \tag{6}$$

The axial force for $30^{\circ} < \alpha < 90^{\circ}$ is calculated in a similar manner as a function of both the axial force that is said to be invariant of angle of attack and a modification for angle of attack. This is shown in Eq. (7).

$$C_A = C_{A,0} \cos^2 \alpha \tag{7}$$

This formulation was empirically derived by Jorgensen (1977). However, the combination of these causes a sharp discontinuity at 30°, the cross-over point. Horton and McDaniel suggest a return to a formulation that more closely follows the physics even to the point of including induced drag. This follows the same idea as the body-to-wind axis transformation that is given by Eqs. (4) and (5). Eqs. (8)–(10) show the formulation in the body and wind axis terminology.

$$C_D = C_{A,0} + kC_L^2 \tag{8}$$

$$C_A = C_D \cos\alpha - C_L \sin\alpha \tag{9}$$

$$C_L = C_N \cos\alpha - C_{A,0} \sin\alpha \cos\alpha \tag{10}$$

Combining these equations while assuming that k = 1, and only keeping normal force coefficient terms that are coupled with axial force coefficients, the formulation becomes

$$\begin{aligned} C_A = C_{A,0}^2 \sin^2\alpha \cos^3\alpha + C_{A,0}\left(\cos\alpha + \sin^2\alpha \cos\alpha\right) \\ -2C_N C_{A,0} \cos^3\alpha \sin\alpha \end{aligned} \tag{11}$$

They show that this new formulation improves the accuracy of the simulation up to about an angle of attack of 45°. They recommend that further work be done in this particular area to further improve the accuracy.

Also as part of this study, they propose a change for the supersonic axial force calculation. In the previous version, the supersonic axial force due to pressure alone is considered invariant of angle of attack in the VDHT method and the hypersonic Newtonian method as implemented. This introduces additional errors when the geometry is at angle of attack. They propose as part of the change to calculate the axial force at each angle of attack to eliminate this discrepancy. A code structure change was suggested to eliminate these angle-of-attack errors. The SOSE theory is also employed but is not affected by the angle-of-attack errors mentioned here.

The most recent revision of Missile DATCOM (version 8/08) was released in 2008. This version included the ability to have nine fin sets with up to eight fins for each set, revised body axial force calculations, and the addition of moment contributions from protuberances. Doyle et al. (2009) discuss the last two upgrades mentioned above. First, the method to calculate the axial force coefficient for bodies with blunted, truncated, and low fineness ratio noses was updated. Second, adding the ability to specify the angular orientation of protuberances enabled the additional of pitching and yawing moment contributions from these protuberances to the total body moments. Changes in the axial force calculation methodology are of great interest. However, since the choice was made not to model the protuberances on the SA-2 missile, the change to implement angular position of protuberances will not be discussed.

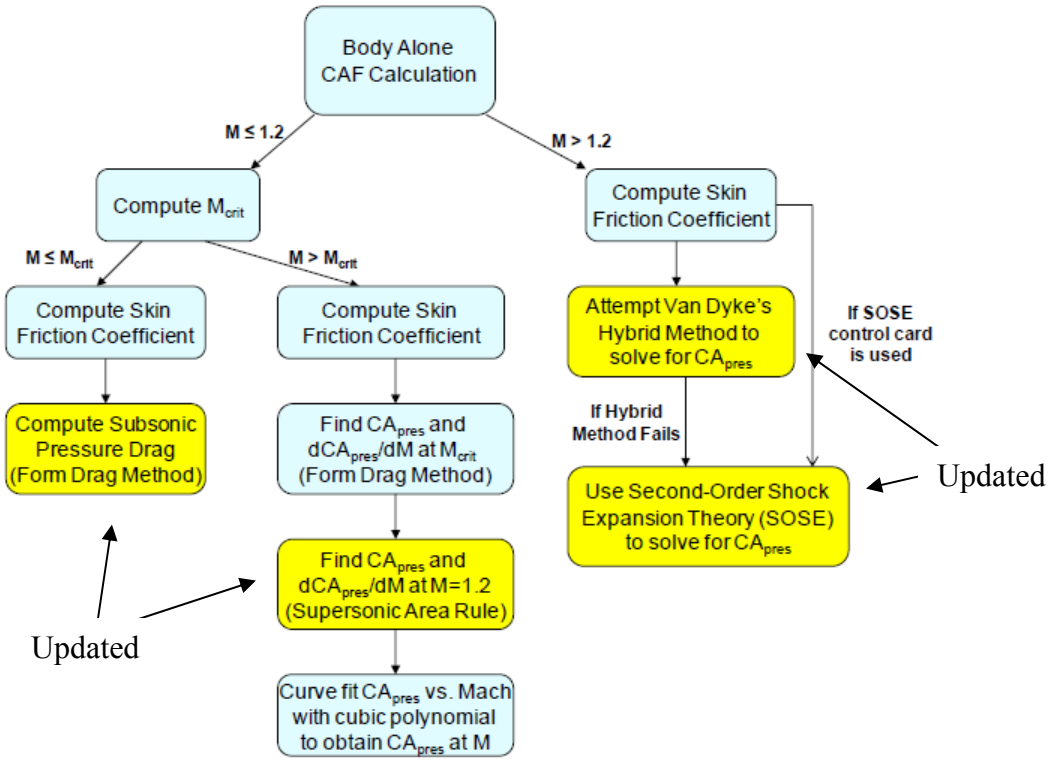

Figure 5. Axial Force Methodology for Missile DATCOM 7/07 (After Doyle, Rosema, Underwood, & Auman, 2009, p. 3)

Figure 5 shows the flowchart for body alone axial force calculations and is marked with the processes that have been updated to increase the accuracy of the aerodynamic predictions. Three areas of related changes are apparent from Figure 5. They correspond to the purely subsonic, the transonic, and the supersonic regions. The delineation between the subsonic and transonic regions is the critical Mach number where supersonic flow is just starting to develop in the flow field, but does not dominate. The delineation between the transonic and supersonic regions is marked at Mach number equal to approximately 1.2. This number almost certainly guarantees that the whole flow field is supersonic with exception of flow in the boundary layer and the flow in regions of separated flow. Different techniques must be employed in these regions due to the different flow physics at play here.

In the 7/07 version of Missile DATCOM, the form drag method is used to calculate the subsonic axial force ($M < M_{crit}$). It is a function of the body fineness ratio. If there is little or no separation, the method produces a good match to actual pressure

drag on the body. However, if there is moderate to severe separation, as seen in nose geometries with low fineness approaching fully truncated, the method severely underpredicts the pressure drag. Based on parametric studies for a range of fineness ratios conducted using CFD, Doyle et al. (2009) proposed a correction that fits a curve to a conical nose factor as a function of fineness ratio and implemented it. This conical nose factor is used in Eq. (12) and (13) to adjust the axial force coefficient.

$$C_{Apres} = ConicalNoseFactor \cdot \left(C_{Apres-trun} - C_{Aform} \right) + C_{Aform} \tag{12}$$

$$C_{Apres-trun} = 0.86 - C_{Afric} \tag{13}$$

As the conical nose factor approaches zero (i.e., for fineness ratios greater than 1.5), the pressure drag component of the axial force approaches the axial force produced by the form drag method alone.

For fully truncated noses, Missile DATCOM 7/07 interpolated between the pressure drag calculated via the form drag method and an empirically determined truncated drag based on the truncation ratio, defined as the truncated diameter divided by the nose base diameter. In a similar manner to the corrections implemented for noses with low fineness ratios, a correction was proposed via a curve fit from parametric CFD studies to correct for the underprediction for this geometry.

In the transonic region (M_{crit} to M=1.2), use of Missile DATCOM 7/07 yielded large differences in the axial force values. The method to determine the pressure component of axial force involves a curve fit of a cubic polynomial to the calculated values of the axial force coefficient. In order to produce this cubic curve fit, one must know the endpoints and slopes at the endpoints. The derivatives are approximated at these endpoints by a finite difference formulation. The M_{crit} endpoint is perturbed by 0.01, and the M = 1.2 endpoint is perturbed by 0.1. The left endpoint follows as a carryover from the subsonic discussion mentioned above. The right endpoint axial force coefficients are both evaluated using the supersonic area rule, which is integrated over the body. The supersonic area rule uses an area for calculations that is the projection of the slice made by the Mach cone angle at a particular point on the plane that is perpendicular to the body axis. Therefore, the area is dependent on both Mach number and the actual cross sectional area. For M > 1.2, VDHT or SOSET is used and a discontinuity develops

because of this switch. The correction proposed for Missile DATCOM 8/08 is to use VDHT and SOSET to calculate the values at the right endpoint for the curve fit, eliminating the erroneously large axial force coefficients that result from using the supersonic area rule when high conical nose half angles are present in the geometry. These changes also eliminate the discontinuity that was present at the right endpoint because of the switch to VDHT or SOSET.

In the purely supersonic region (M > 1.2), the 7/07 version of Missile DATCOM uses both VDHT and SOSE. VDHT is used until its applicability ends and the program abruptly switches to SOSE. The end of the applicability of VDHT occurs when the slope of the body at any point is greater than the Mach cone angle calculated from the freestream Mach number. This switch causes a distinct discontinuity. To resolve it, Doyle et al. (2009) propose a smoothing routine that interpolates between VDHT and SOSET for a particular nose fineness ratio as a function of Mach number. Figure 6 gives an excellent graphical representation of this interpolation scheme.

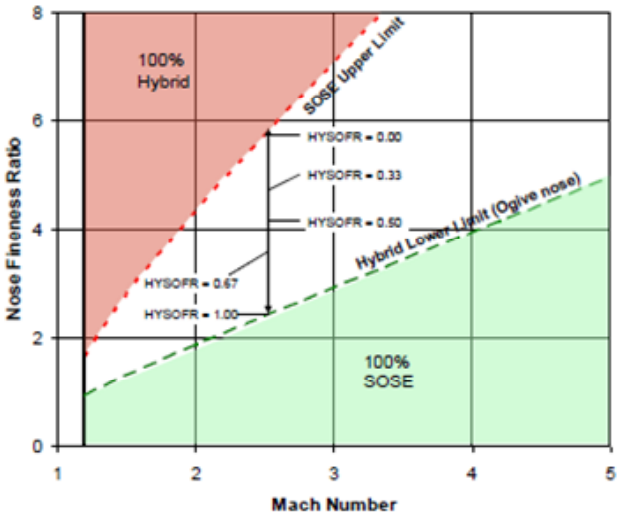

Figure 6. Graphical Representation of Interpolation Scheme for Axial Force in the Supersonic region for Missile DATCOM 8/08 (From Doyle, Rosema, Underwood, & Auman, 2009, p. 10)

II. GEOMETRY MODELING AND RESEARCH APPROACH

A. GEOMETRY MODELING

1. Missilelab

a. Interface with Missile DATCOM

Missilelab, developed by Auman et al. at the United States Army Aviation and Missile Research, Development, and Engineering Center (AMRDEC), provides a convenient interface for many aerodynamic prediction software packages including Missile DATCOM (AMRDEC and AFRL Wright Patterson AFB). Figure 7 shows a solid model representation of the SA-2 missile with three fin sets (canards, wings, and control surfaces from nose to tail, respectively). A side view of the modeled SA-2 missile is shown in Figure 8.

Figure 7. SA-2 solid rendition from Missilelab

A series of input tabs within the geometry section of Missilelab is provided for each of the major components of a general missile design (nose, body, fins, afterbody, protuberances, etc.) Parameters for these components are input, and a model of the geometry quickly emerges like those in Figures 7 and 8. No knowledge of solid modeling using CAD software is necessary. The most important advantage of this type of synthetic modeling method is the fact that the user does not need to know how to create the geometry input file for the particular aerodynamic prediction software.

b. Modeling Trade-offs

Because the new geometry provided by MSIC did not include the airfoil profiles, the standard double circle arc airfoil was used for all of the airfoil sections of the fins. The lengths of the fins are given and the thickness of the root and tip sections were assumed to be 2% of their respective chord dimension. Table 2 gives the resulting dimensions for the fins. Fin-Set 1 comprises the canards. Fin-Sets 2 and 3 comprise the wings (2 is the upper and 3 is the lower). Fin-Set 4 comprises the tail-fins (control surfaces).

Fin Set	Root Chord	Root Thickness	Tip Chord	Tip Thickness	Semi-span	LE sweep angle	TE sweep angle
1	0.193	0.0097	0.046	0.0023	0.105	43.89	-23.66
2	1.7724	0.045	0.3842	0.0159	0.8215	55.96	-11.84
3	1.7724	0.035	0.2692	0.0127	0.8707	56.64	-11.73
4	0.447	0.0206	0.111	0.0064	0.5374	27.77	-5.83

Table 2. Modeled fin dimensions (dimensions in meters, angles in degrees; positive sweep is towards the rear of the tail of the missile)

Figure 8 shows the side view of the modeled missile geometry. The three grouping of fins (canards, wings, and tails) have four fin panels, one each at 45°, 135°, 225°, and 315°. This resembles a cross that is rotated 45°.

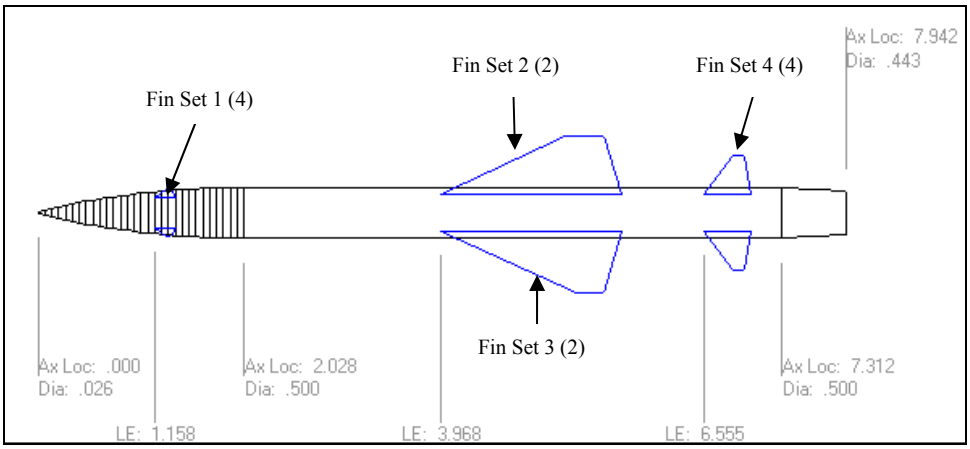

Figure 8. Modeled missile geometry with major dimensions (meters)

2. Solid Modeling for CFD Domain

The solid model for use in the CFD calculations was created in Solidworks Education Edition SP5.0. Figure 9 shows the missile body and fins. The missile body consists of a series of extrusions (tangent ogive nose, cylindrical body, and conical boat-tail). The fins were created by drawing the airfoil shapes for the root and wing tip and producing a loft between them. For each set, only one fin was created, while all of its twins were created by mirroring it in a pattern about the body axis. Once the solid model for the missile was created, it was removed from the fluid domain by a process of subtraction. This leaves only the surface of the missile and the surrounding fluid for discretization to be used by the CFD solver.

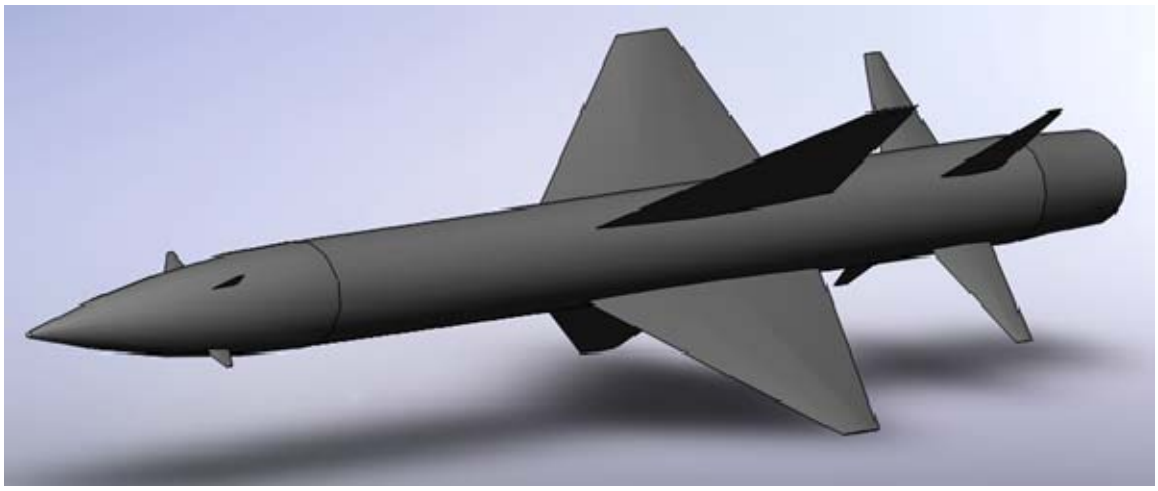

Figure 9. SA-2 missile solid model created in Solidworks 2008

3. Computational Domain Characteristics and Computing Resources

The computational domain is a parallelepiped with physical dimensions of 6.34 m (y) by 6.34 m (z) by 32 m (x). The missile body is located 8 meters from the inlet of the domain, a distance of approximately 16 characteristic lengths (missile diameter). The domain extends past the tail to the outlet approximately 32 characteristic lengths. The sides extend approximately six characteristic lengths in both the y and z directions away from the missile body. The computational grid has 345,484 nodes with 1,703,985 elements. Seven inflation layers were added on the surface of the body to better capture boundary layer physics. The full domain was modeled in lieu of utilizing a smaller

domain with symmetry planes because the original intention for this part of the study was to simulate changes in the angle of attack for the missile. However, this part of the analysis was ultimately not performed. The fluid dynamic computations using the discretized domain were carried out on the NPS/MAE cluster computer, a Unix-based computing platform with 32 nodes and 4 processors per node.

B. EXPERIMENTAL DATA

Data for this study were provided by MSIC/Defense Intelligence Agency. The data set consists of some wind tunnel data and modeled data generated using MATLAB/Simulink. However, all the data are deemed to be from an experimental source. The full details of the experimental procedures that were used to produce this data set are not available. Equation (14) summarizes the inputs given for the total axial force coefficient. Data for normal force and moment coefficients including their derivatives are also given as part of the data set.

$$C_A = C_{A,0} + C_{A,\alpha} + C_f + C_{A,\delta} \tag{14}$$

These data and a similar geometry were studied previously by Teo (2008) using Missile LAB code. However, the missile geometry then was set up from a rudimentary drawing and not one that represented a high fidelity version as used in the present study. Unavailable dimensions were scaled off the drawing as best as possible. Additionally, certain details of the SA-2 missile's construction were not visible in the drawing and for such situations; the fidelity level is less in the calculations. The differences with the prototype included airfoil cross-sections and the presence of a boat-tail on the second stage housed within the first stage. Updated geometry drawings were subsequently provided by MSIC for this particular study that included protuberances and the aforementioned boat-tail. Reasonable guesses were made for the airfoil cross-sections.

It is unclear whether boundary layer trips were used on the model to fix the transition onset point to better match the flow characteristics of the full-scale missile. Early results generated in the study lead to the surmise that boundary layer trips were used during testing. Thus, in Missile DATCOM calculations, the boundary layer is assumed to be fully turbulent.

C. RESEARCH APPROACH

Parametric studies of the missile performance were conducted using Missile DATCOM to produce data for comparison with the range of flow conditions included in the MSIC data. A large amount of data for many different flight conditions have been computed. Most of the Missile DATCOM output was produced for specific values of Mach number, angle of attack, control surface deflection, and flight altitude for which the MSIC data were provided. If anomalies were noticed, other flight parameters were used to investigate the workings of Missile DATCOM.

CFD analysis is also included in this study to see how the results from these types of simulations can compare. Complete agreement between these computational tools may not be possible, but seeing some similarities may give good insight into the ability to use both Missile DATCOM and CFD as powerful design tools.

D. TEST CONDITIONS

The test conditions were chosen to correspond with the data provided by the sponsor. All of the cases were shown in this study were calculated with forced turbulent flow. Natural transition was briefly investigated, but it was found to have little effect on the output values since laminar flow accounts for a very small portion of the flow regime at the high Reynolds numbers studied. Table 3 lists the nominal conditions used.

Mach Numbers	**0.8, 1.2, 1.6, 2.0, 2.5, 3.0, 3.5, 4.0, 4.5**
Angles of Attack	0º–24º (in 2º increments)
Altitudes	0 m, 5000 m, 10000 m, 20000 m, 30000 m
Surface Roughness	0 cm, 0.001016 cm, 0.003048 cm

Table 3. Test conditions

THIS PAGE INTENTIONALLY LEFT BLANK

III. PRESENTATION OF RESULTS

A. MOTIVATION FOR FURTHER STUDY FROM THE RESULTS OF PREVIOUS WORK

The initial motivation for the study came from a need to extend the previous studies to other flight conditions involving fin deflections and for different altitudes. It was also felt that the differences between the computations and experiments at transonic flow conditions warranted additional study. Figure 10 compares the experimental data with results from using the first geometry supplied by MSIC with Missile DATCOM 7/07 and the updated geometry with Missile DATCOM 8/08.

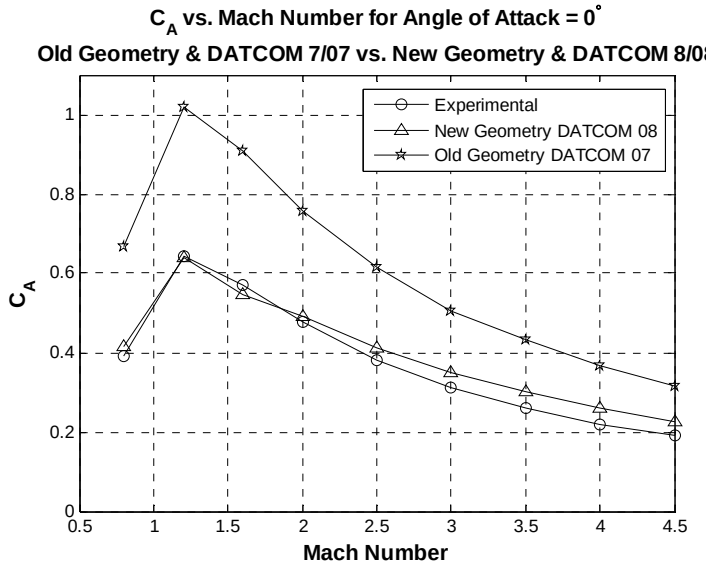

Figure 10. Comparison of C_A for calculations performed using the old geometry with DATCOM 7/07 and those using the new geometry with DATCOM 8/08

The improvement obtained from using the latter in the degree of agreement between computations and experiment is striking. Thus, a repeat study of the missile with the newer code was undertaken for flight conditions that included fin deflections.

B. MISSILE DATCOM 7/07 AND MISSILE DATCOM 8/08

Chapter I, Section E, mentioned recent changes to Missile DATCOM. One particular change is to the method in which the pressure component of the axial force is

computed. The following discussion shows that, indeed, there has been a major change from 7/07 to 8/08 and it confirms considerable improvements in accuracy that were obtained in the range from M_{crit} to M = 1.2. Figure 11 shows the mismatch that exists between the 7/07 and 8/08 versions in this range.

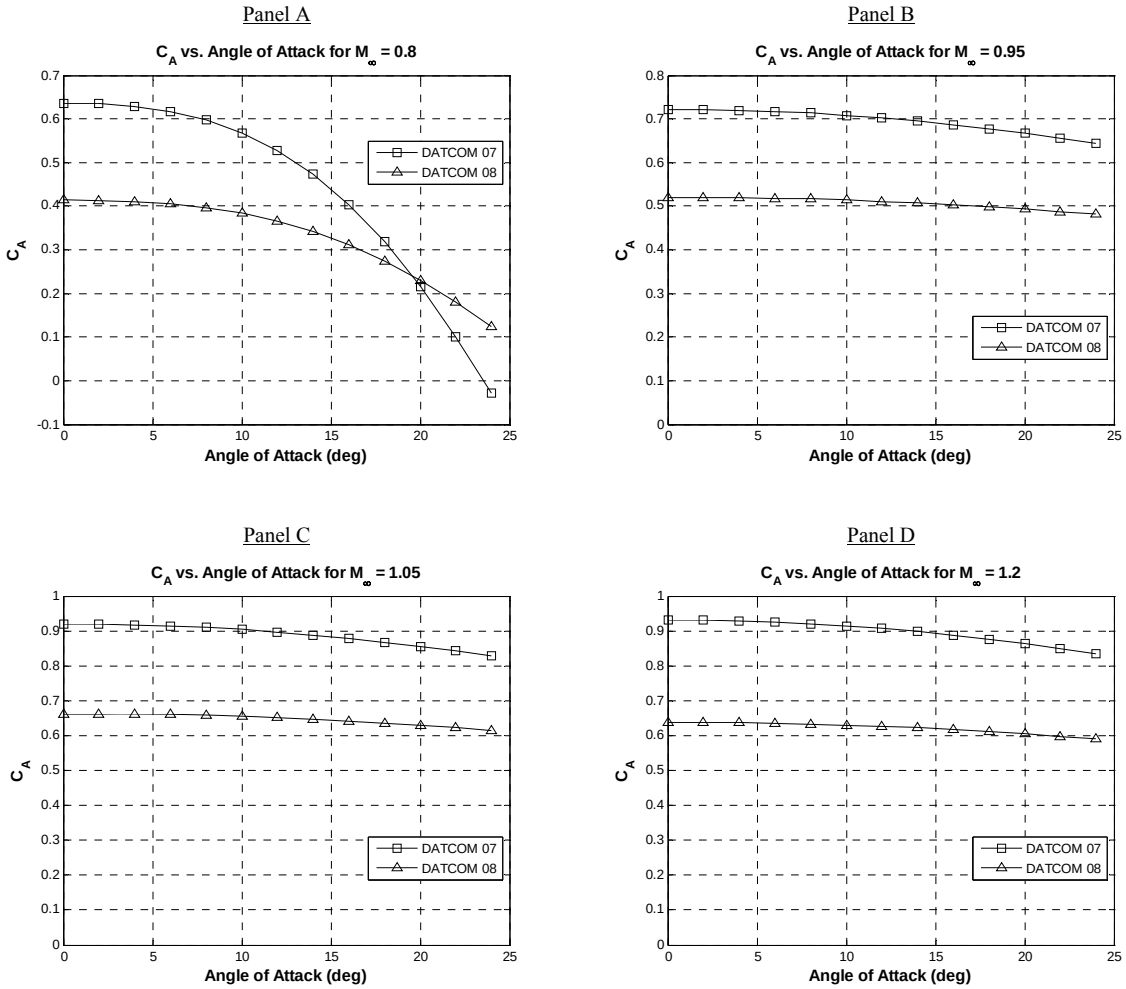

Figure 11. C_A vs. Angle of Attack for Missile DATCOM 7/07 and Missile DATCOM 8/08 for M = 0.8, 0.95, 1.05, and 1.2

It is easy to see in three of the four panels of Figure 11 that Missile DATCOM 7/07 overestimates C_A compared to Missile DATCOM 8/08. However, something interesting happens in panel A at M = 0.8. This is near the critical Mach number. The graphs cross at approximately 20° and the value of C_A at 24° becomes negative, which implies a thrust and not drag. Whereas it is unclear why a negative C_A value was computed, the non-negative C_A value of 8/08 code is clearly more acceptable. The

negative value that is seen at 24º is an anomaly that is obviously not present anywhere in the full range of experimental values provided by MSIC.

In Figure 11, we can see the definite difference between the two versions of Missile DATCOM. The better test of how the new improvements have affected the output is to compare each to the MSIC data. Figure 12 shows the comparison at M = 0.8 and M = 1.2. Notice that Missile DATCOM 7/07 considerably overestimates C_A (in panel A, less than 20°) whereas the agreement for Missile DATCOM 8/08 is quite good. Thus, it was decided to make all comparisons with the latest version of Missile DATCOM.

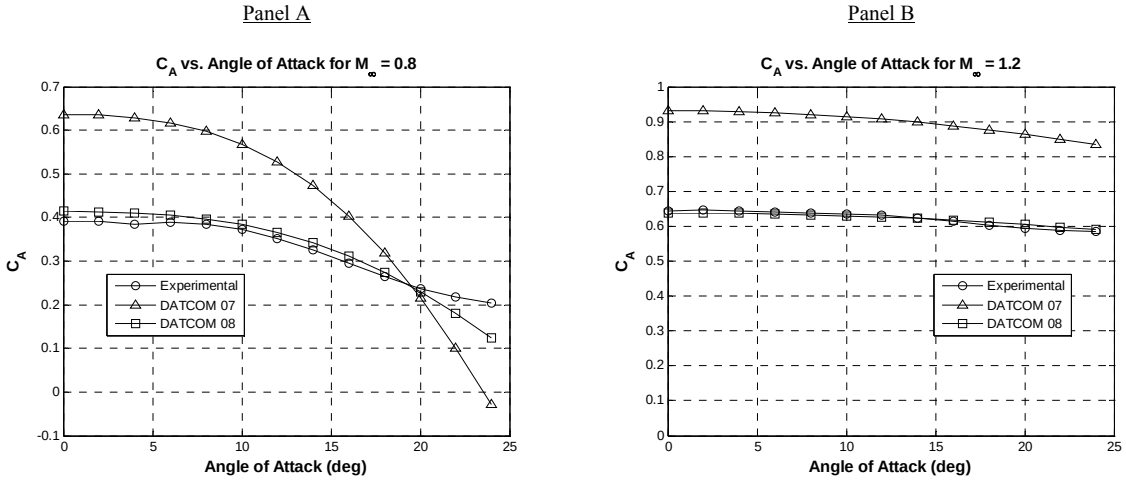

Figure 12. C_A vs Angle of Attack for MSIC Data, Missile DATCOM 7/07, and Missile DATCOM 8/08 for M = 0.8 and 1.2

Figure 13 highlights the variation of C_A and the differences between Missile DATCOM 7/07 and Missile DATCOM 8/08 as a function of Mach number at 0º and 20º angle of attack. Again, the disparity between these two versions is easily quantifiable. The changes made to Missile DATCOM between the 7/07 and 8/08 versions for this range of Mach numbers was certainly a significant improvement. MSIC data is shown for M = 0.8 and 1.2 as a reference. No MSIC data exists between the points shown in Figure 13. Therefore, the line shown between the points is dotted to indicate only a possible fit. The better fit in this region can be attributed to recent improvements in the transonic computations performed by Missile DATCOM.

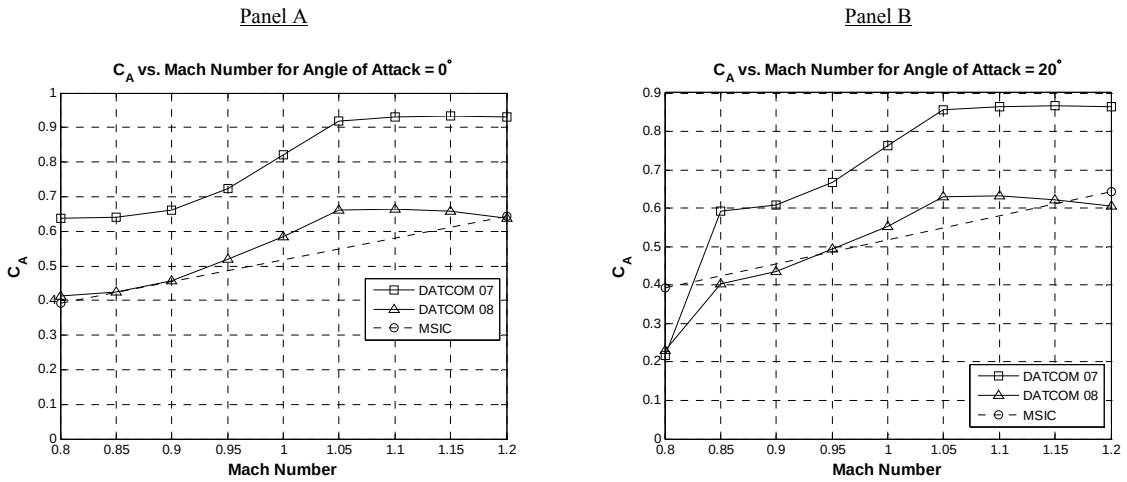

Figure 13. C_A vs Mach Number for Missile DATCOM 7/07 and Missile DATCOM 8/08 for Angle of Attack 0° and 20° including MSIC data at M = 0.8 and 1.2 for comparison

C. AXIAL FORCE COEFFICIENT

1. Axial Force Coefficient as a Function of Angle of Attack

Parametric studies were conducted using Missile DATCOM for M = 0.8 to M = 4.5 and 0º angle of attack to 24º at the same intervals as the data provided by MSIC. Figures 14–22 give a survey of the results of these studies and percentage differences found between the computed Missile DATCOM output and the data provided by MSIC. These particular cases were run forcing turbulent flow with a surface roughness of 0.001016 cm, which was found by Teo (2008) to give good results.

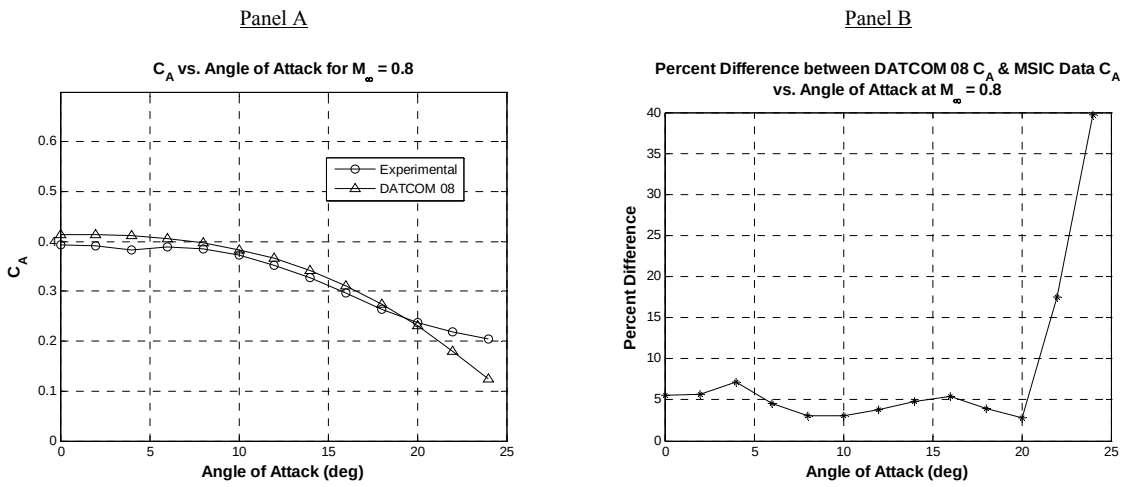

Figure 14. C_A vs. Angle of Attack for MSIC Data and Missile DATCOM 8/08 for M = 0.8

Figure 14 shows approximately 5% difference between the MSIC data and Missile DATCOM 8/08 over a large range of angle of attacks, which was deemed excellent. However, after an angle of attack of 20º the agreement breaks off and the results diverge considerably. It is not entirely clear why this discrepancy appears other than that this is a high angle of attack case. One possible explanation is likely the well known differences in the formation and evolution of the forebody vortices at these high angles of attack on an axisymmetric slender body.

Since the SA-2 missile traverses through this Mach number for less than 10 seconds, additional attention was not devoted to this discrepancy. Most of the flight envelope encompasses the supersonic regime that extends up to about Mach 3. Thus, studies at lower Mach numbers are not of interest for this missile. However, it does show that for low to moderate angles of attack at this particular Mach number Missile DATCOM 8/08 is able to provide excellent results that would be adequate for preliminary design studies.

Figure 15 shows the best agreement, over the widest range of angle of attacks, from among Figures 14–18 of this section and Figures 32–35 of Appendix C. The maximum difference occurs at 20º and shows only a 2% difference. This level of

agreement, for this particular Mach number, indicates that in this region, Missile DATCOM provides predictions that accurately model the physics.

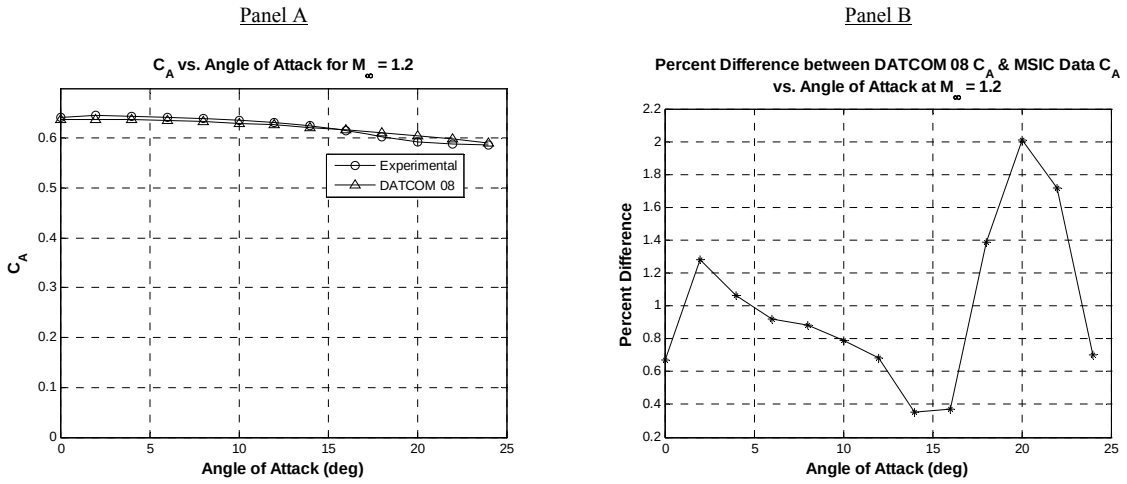

Figure 15. C_A vs. Angle of Attack for MSIC Data and Missile DATCOM 8/08 for M = 1.2

Figures 16–18 show a noticeable difference in the general trend between the MSIC data and DATCOM output as the angle of attack is increased. Although apparently opposing trends are observed, it should be noted that in Figure 18 an agreement of better than 10% exists for most of its range and Figures 16 and 17 show an agreement better than 10% for angles of attack of 17° or less.

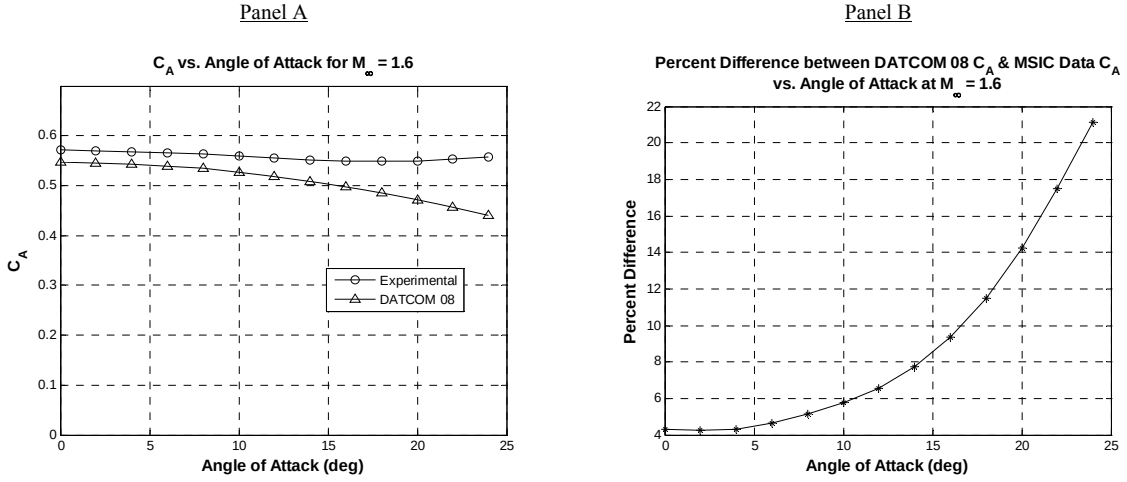

Figure 16. C_A vs. Angle of Attack for MSIC Data and Missile DATCOM 8/08 for M = 1.6

Panel A

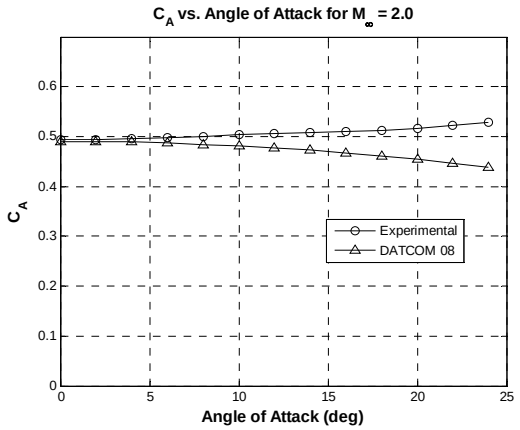

Panel B

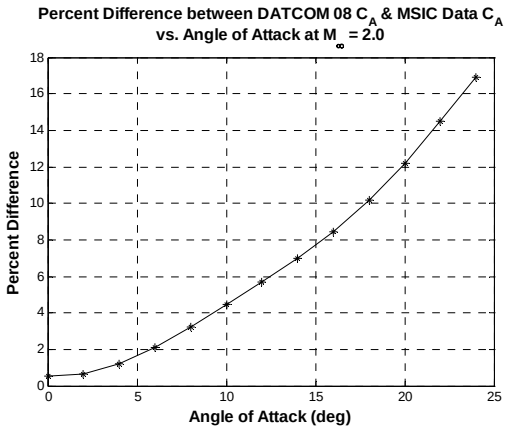

Figure 17. C_A vs. Angle of Attack for MSIC Data and Missile DATCOM 8/08 for M = 2.0

In general, this level of agreement is considered satisfactory in missile compuatations using empirical codes so, it is accepted. The code used is known to produce results of less than 10% difference if the predictive region of interest is limited to an angle of attack of approximately 20°.

Panel A

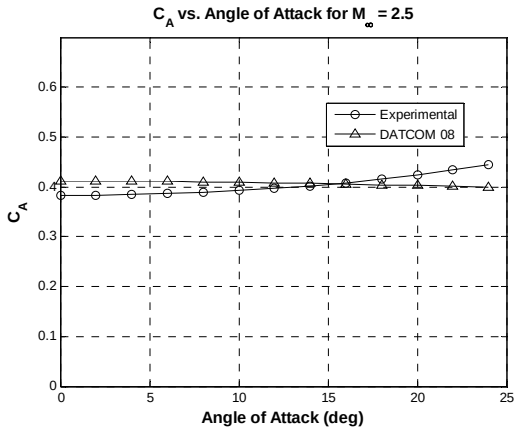

Panel B

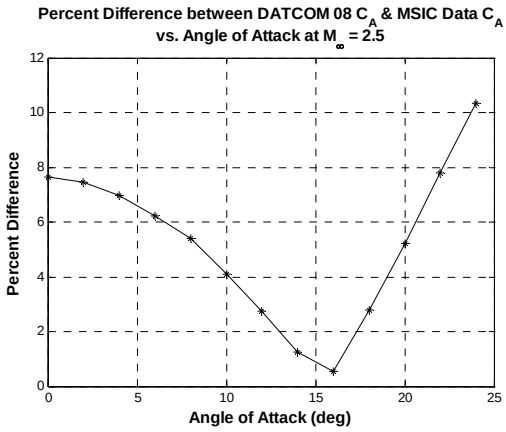

Figure 18. C_A vs. Angle of Attack for MSIC Data and Missile DATCOM 8/08 for M = 2.5

Differences seen in the plots presented beyond 20º can naturally be expected to be larger because of this artificial restriction in the predictive range of Missile DATCOM. This indicates that the code is most suitable if the flight envelope consists of normal course and altitude corrections, which limits the ability to accurately predict the aerodynamic forces in any radical maneuver.

For Mach number > 3.0, the trend in both the MSIC data and DATCOM output are both monotonically increasing and concave upward. This is shown in Figures 32–35 of Appendix C. A likely explanation for the change in the trend and the overpredictive/underpredictive nature that is seen from the output of DATCOM from this point onward is a change in the computational method used around Mach 3.0. Additionally, we can say that for Mach numbers above 3.0 the accuracy meets the goal of less than 10% at angles of attack greater than approximately 10º. Overall, the average difference for C_A is approximately 7%.

2. Axial Force Coefficient as a Function of Mach Number

Although the data presented here are identical to what was presented in Chapter III, Section C.1, an alternate view—in this case as a function of Mach number for a representative sample of angles of attack—reinforces the conclusions made in the previous section.

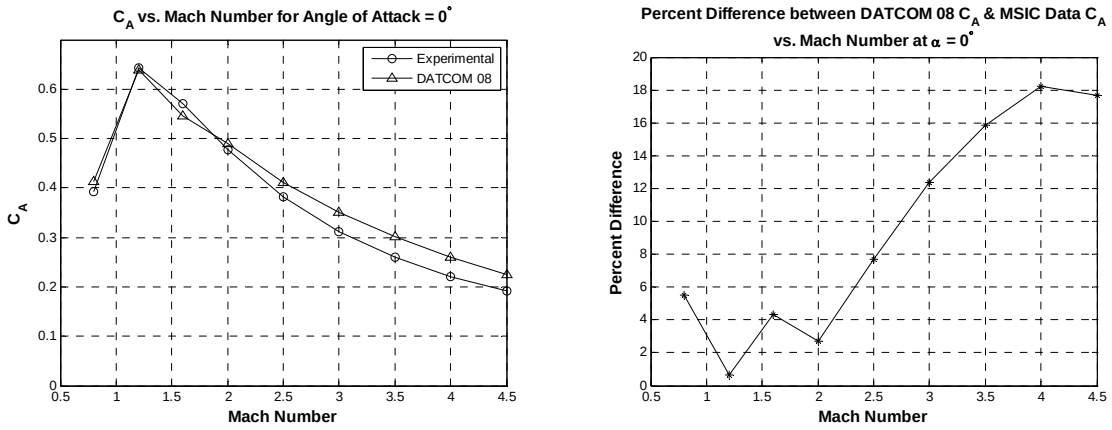

Figure 19. C_A vs. Mach Number for MSIC Data and Missile DATCOM for Angle of Attack = 0º

In Figures 19 and 20, the desired accuracy goal is met for approximately Mach 3.0 and below. Figure 21, however, shows the opposite behavior. For large angles of attack, the relationship is reversed. The higher the Mach number, the better the accuracy becomes.

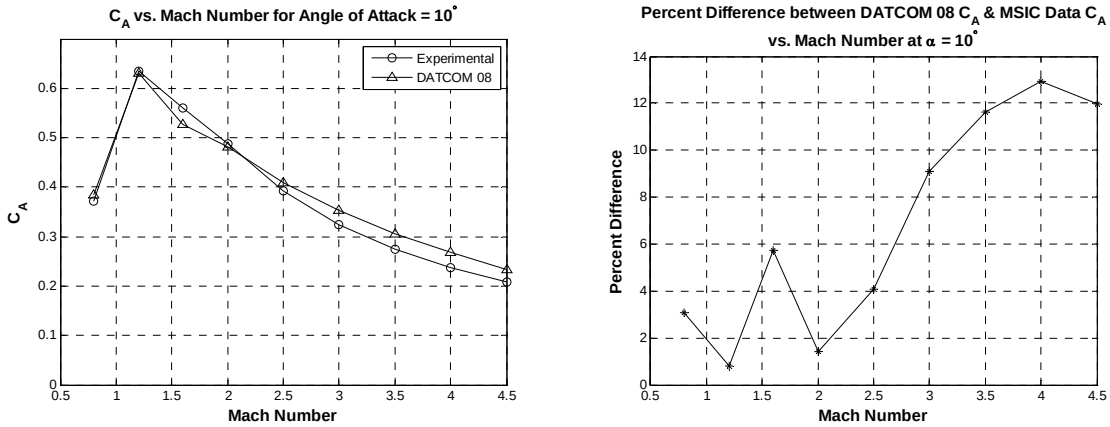

Figure 20. C_A vs. Mach Number for MSIC Data and Missile DATCOM for Angle of Attack = 10º

The same conclusion can be reached when analyzing this data as a function of angle of attack. A general framework then arises that places a lower and upper bound on the prediction domain to maintain the desired accuracy. For Mach numbers less than approximately 3.0, it can be expected that an accuracy of ±10% is possible for angles of attack less than approximately 18º (see Chapter III, Section C.1). Conversely, for Mach numbers greater than this value, the accuracy of ±10% can be expected for angles of attack higher than approximately 18º.

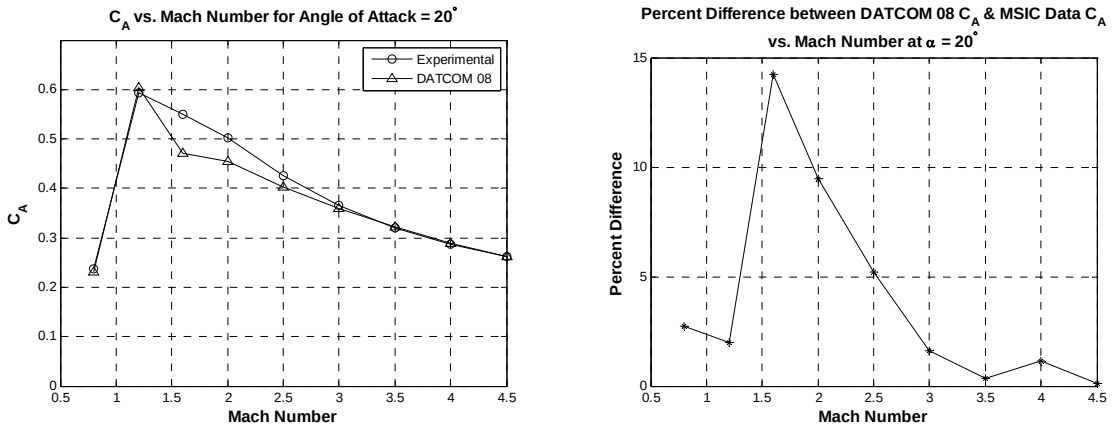

Figure 21. C_A vs. Mach Number for MSIC Data and Missile DATCOM for Angle of Attack = 20º

D. SKIN FRICTION

As stated earlier, all Missile DATCOM calculations for this parametric study of the coefficient of skin friction are run as purely turbulent cases. While agreement in C_A falls within the tolerance goal, it may be entirely possible that the individual components (C_f, C_{A0}, etc.) will not match those derived from experiments. This is because of the issues involved in measuring skin friction over the model at the various Mach numbers of interest. If success can be achieved, then use of Missile DATCOM to calculate all the components would enable it to be a more powerful tool. Figure 22 shows the comparison between the MSIC data and Missile DATCOM 8/08 C_f calculations. The code has overpredicted the C_f values. The roughness value for the MSIC data is not known. Even though turbulent, the surface was treated as aerodynamically smooth (roughness = 0 cm) for the Missile DATCOM calculations. Consequently, one conclusion can be drawn. With the limited details of the missile and data in hand, one cannot perform better calculations to get a good agreement because the roughness cannot be reduced any further in Missile DATCOM.

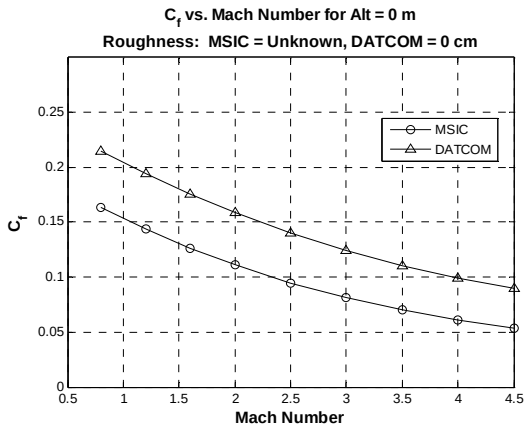

Figure 22. C_f vs. Mach Number for MSIC data and Missile DATCOM 8/08 at Sea Level

The output for C_f at altitudes other than sea level is available in Figure 36 of Appendix C. The overall trends are identical to Figure 22. Although the agreement for C_f is not the desired objective, the Missile DATCOM output can still be used to get a general idea of the magnitude and the behavior of the skin friction coefficient as a function of Mach number. Being able to predict C_f trends is by itself valuable at these high angles of attack, altitudes and speeds, since the flow Reynolds number changes over a significant range. Data for the skin friction coefficient were only given at zero angle of attack. No discussion of the changes of skin friction with angle of attack will be made.

E. CONTROL SURFACE DEFLECTIONS

In a supersonic missile, the control surfaces are small compared to the overall size of the missile. However, it can be expected that small deflections can produce large changes in the missile orientation because of the comparatively large forces produced as a result of the high speed of the body. Hence, the present study used fin deflection angles up to 10^o. Figures 23–26 show the result of the parametric study conducted for the SA-2 missile geometry using Missile DATCOM and its comparison with the MSIC data for Mach numbers 1.2, 2.0, 2.5, and 3.0. Each of these Mach numbers is presented with control surface deflections of 5^o and 10^o.

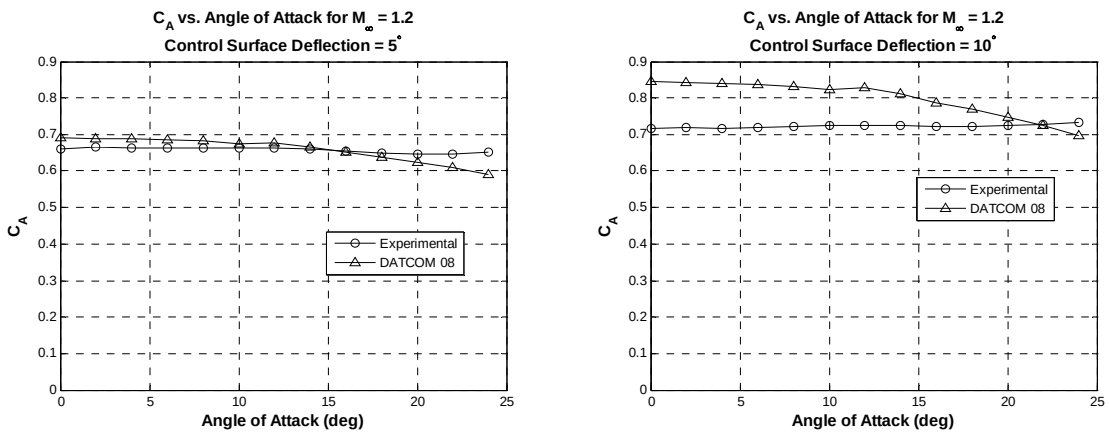

Figure 23. C_A vs. Angle of Attack at M = 1.2 for control surface deflections of 5º and 10º

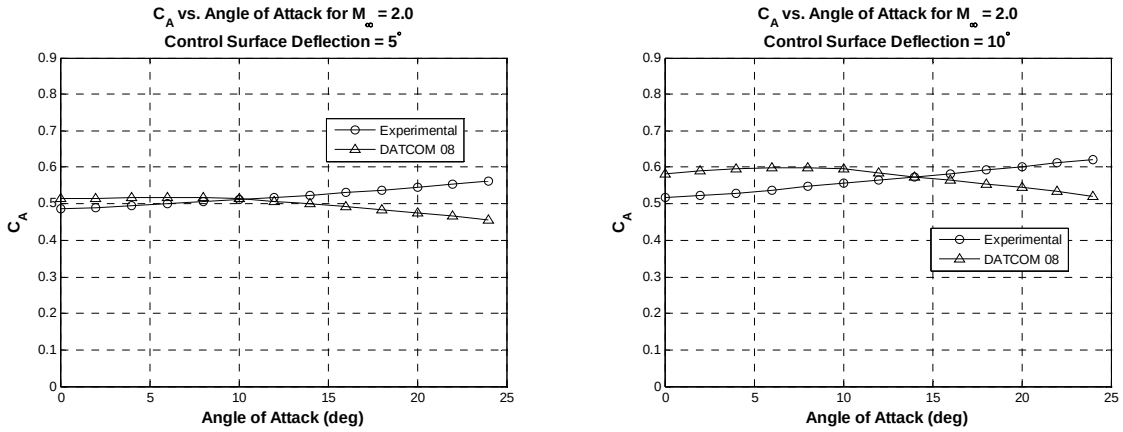

Figure 24. C_A vs. Angle of Attack at M = 2.0 for control surface deflections of 5º and 10º

Figure 37 of Appendix C shows the results for the Mach numbers 0.8, 1.6, 3.5, 4.0, and 4.5 for the same control surface deflections presented in Figures 23–26. Although small differences are seen, Missile DATCOM produces values that have relatively good correlation with the MSIC dataset for the smaller deflection angle of 5º. The difference, as can be expected, increases for 10º but is still in an acceptable range. For preliminary designs, these calculations would give rough estimates for the contribution of these fins during maneuvers and the extra thrust required to counteract their effect.

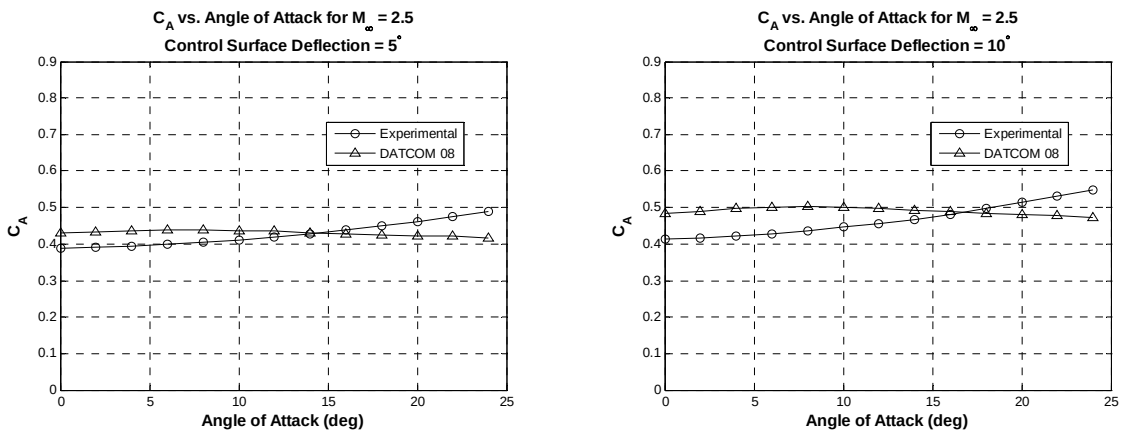

Figure 25. C_A vs. Angle of Attack at M = 2.5 for control surface deflections of 5º and 10º

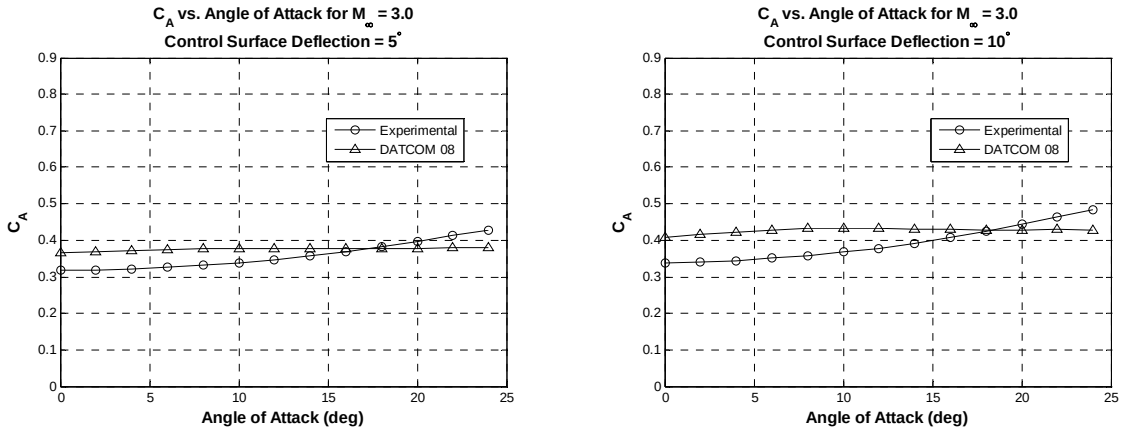

Figure 26. C_A vs. Angle of Attack at M = 3.0 for control surface deflections of 5º and 10º

Table 4 gives a tabulation of the average percent difference for the entire body of test conditions utilized. For all given Mach numbers on average, as control surface deflection angle is increased by 5º the difference increases to approximately 1.5 times the previous level.

Control Surface Deflection Angle (deg)	Average Percent Difference (%)
5	8.99
10	13.42
15	20.09
20	48.93
25	77.66
30	53.90

Table 4. Average percent difference in C_A for control surface deflection angles 5º–30º

The differences documented here lead to the inference that when using Missile DATCOM for parametric studies, involving control surface deflections, the maximum deflection should be limited to approximately 10º. This will ensure that a large error is not realized with an untested design. For the case of a supersonic missile, this certainly would be adequate information for a first approximation to size the engine.

No parametric studies were conducted for purely subsonic conditions, so a projection for the level of agreement that might be present if studies were performed on subsonic missiles (e.g., cruise missiles) is not possible.

F. NORMAL FORCE COEFFICIENTS

Sections C and E present the data and show the level of agreement that exists in the axial force coefficient between the MSIC data and the output of Missile DATCOM 8/08 over a wide range of Mach numbers, angles of attack, and a limited range of control surface deflections. Numbers greater than the targeted average of 10% absolute difference are noticed in the axial force coefficient. It is of interest to determine the level of comparisons with the normal force coefficient.

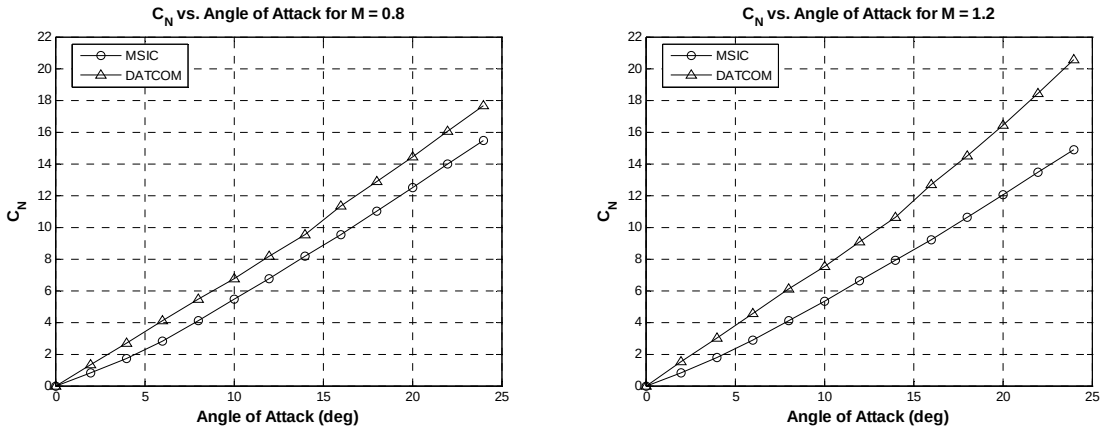

Figure 27. C_N vs. Angle of Attack for M = 0.8 and 1.2

Figures 27–29 compare the MSIC data and the Missile DATCOM output for Mach numbers 0.8, 1.2, 2.0, 2.5, and 3.0. These flight conditions were chosen as representative values of the flight envelope for the SA-2 missile. Additional flight conditions are available as Figure 38 in Appendix C. It is evident that as the Mach

number is increased, the difference reduces. At Mach 4.5 (Figure 38 of Appendix C) the average difference approaches approximately 12%. The average difference in the typical flight envelope of Mach 1.2 to Mach 3.0 ranges from approximately 31% to approximately 16%. While this difference is beyond the less than 10% difference target, it shows a consistent decline in over the Mach number range for the full range of angles of attack. This knowledge may serve as a basis to correct the predicted aerodynamic coefficients of an unknown configuration of similar missile geometry in the typical flight envelope.

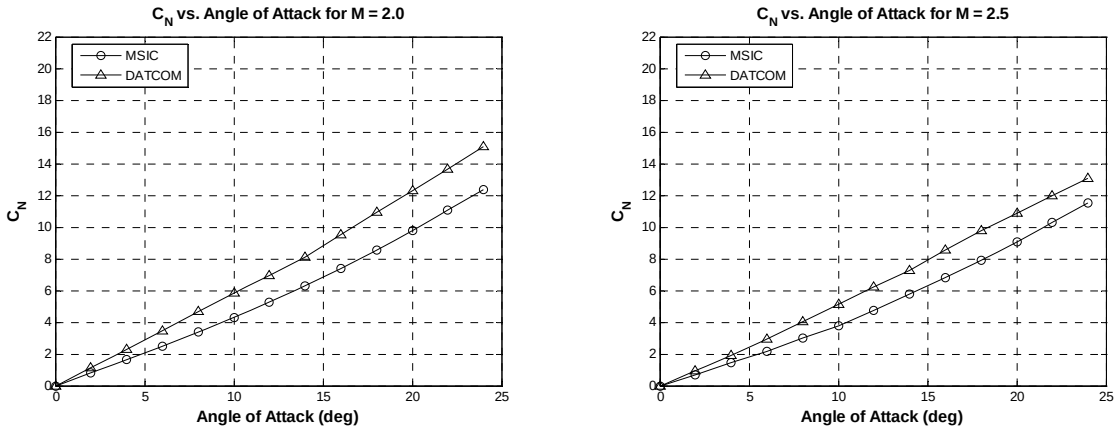

Figure 28. C_N vs. Angle of Attack for M = 2.0 and 2.5

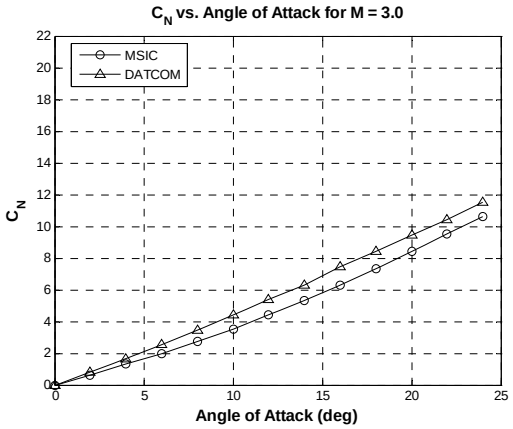

Figure 29. C_N vs. Angle of Attack for M = 3.0

In Figures 27–29, the predicted to experimental level agreement decreases as the angle of attack is increased. Missile DATCOM consistently over predicts the normal force coefficient. This over prediction in the computations can likely be contributed to

the inability to accurately model the flow physics, which is naturally extremely complicated. The asymmetric nature of the vortical flow structures that are attached to the body and are also shed from the body create unsteadiness in the flow that cannot be modeled. While the formation of these vortices on the body and fins increase the theoretical lift, the asymmetric nature of their formation acts to reduce the amount of additional lift that can be produced. This is shown as a lower sloped distribution for the MSIC data than that predicted by Missile DATCOM. However, this inability to accurately model the physics of the flow can be corrected by the error correction proposed as Eq. (15) between Mach 1.2 and 3.0.

$$C_N^{act} = ErrCorr \cdot C_N^{calc}$$
$$ErrCorr = 0.016255M^4 - 0.10744M^3 + 0.23219M^2 - 0.096145M + 0.62297 \quad (15)$$

The error correction is a fourth-order curve fit to the average percent differences at distinct points between Mach 1.2 and 3.0. Figure 30 shows the effect of adding the correction for the angles of attack of 2º, 10º, and 20º for the range of Mach numbers in question. For angles of attack less than 6º the correction does not produce results that meet the goal of less than ±10% difference. However, from 6º on, the error correction produces corrected Missile DATCOM values that have less than 9% difference. Because this error correction is derived from only one missile configuration, it can only be used for the SA-2 or similarly configured geometries. Further study of other configurations is necessary to produce a more general correction.

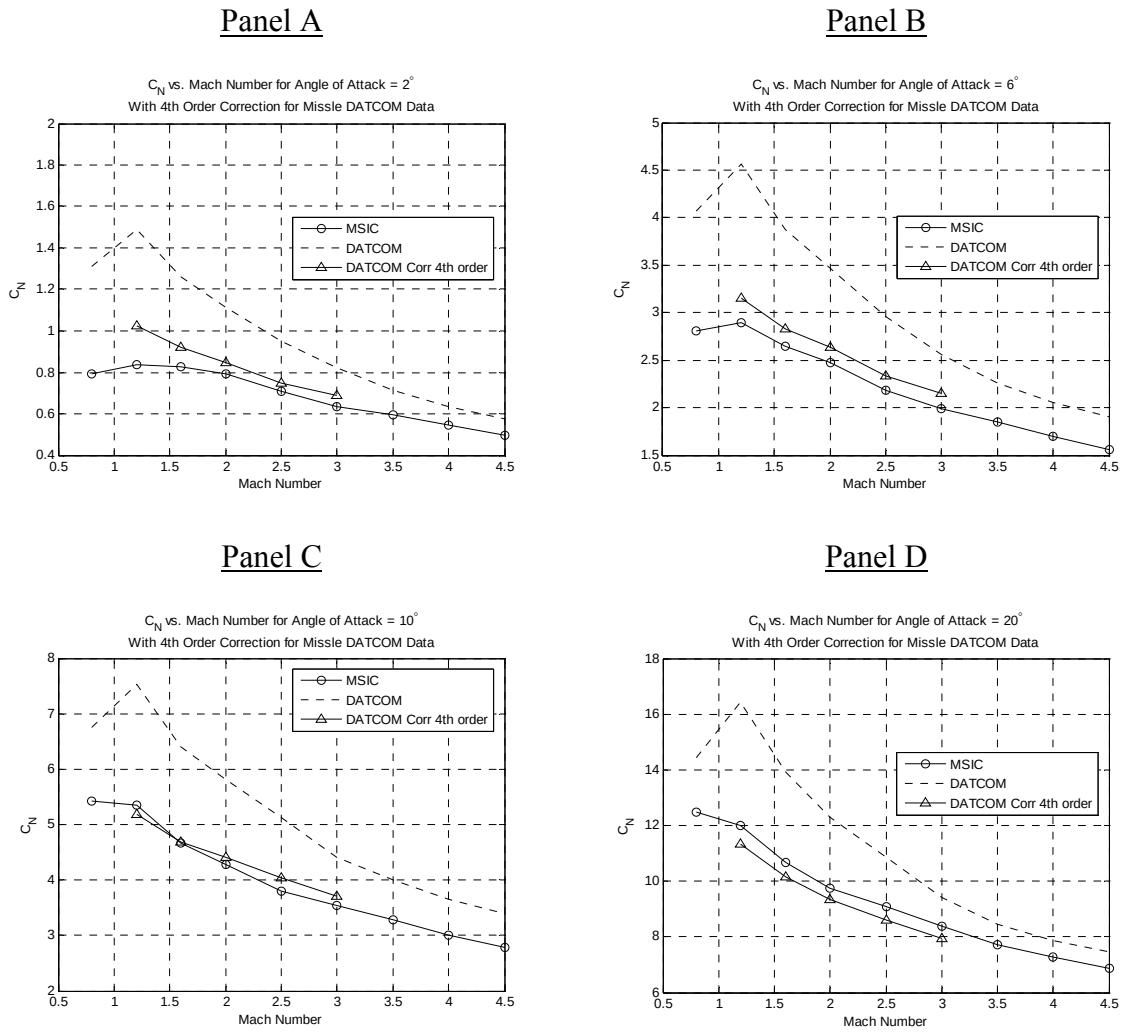

Figure 30. C_N vs. Mach Number for Angles of Attack of 2º, 6°, 10º, and 20º with a 4th order correction

G. CFD COMPARISONS

ANSYS CFX was chosen as the compressible solver for completing the CFD analysis for the SA-2 Missile. Parametric studies from Mach 0.2 to Mach 2.5 were conducted. This range of Mach numbers far exceeds the normal flight envelope into the low subsonic region. However, these subsonic solutions were used to seed the supersonic solutions. The upper Mach number for the range studied is near the top of the operational envelope but does not reach the approximate ceiling (M = 3.0). Solutions above this

Mach number were attempted but resulted in unstable simulations, and thus, the computations are limited to the lower Mach number values. The standard k-ε turbulence model was employed in these calculations.

Figure 30 shows the comparison of the axial force coefficients for an angle of attack of 0º from the three sources: MSIC, Missile DATCOM, and CFD. The excellent agreement between the Missile DATCOM data and the MSIC data has been discussed previously. The CFD data, however, does not show the same promising agreement. The CFD data shown was calculated for an aerodynamically smooth body. In addition to the 0.001016 cm roughness, output from Missile DATCOM is shown for an aerodynamically smooth body.

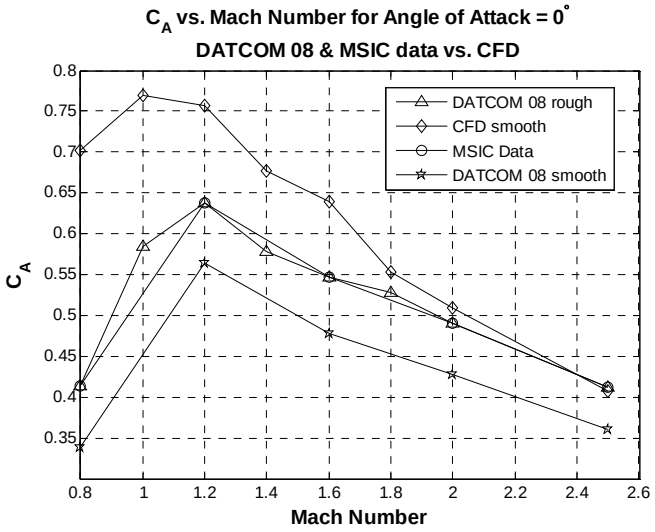

Figure 31. C_A vs. Mach Number for MSIC data, DATCOM 08, and CFD

As can be seen, the differences between the results from CFD and Missile DATCOM vary from approximately a difference (with respect to DATCOM 08 smooth) of 108% at M = 0.8 to 13% at Mach 2.5. The curves have similar shapes, which is promising despite the large difference. The "transonic drag rise" is present as well. Thus, we can say that the physics being modeled for each of the computational tools are similar. More study is required to determine whether a CFD simulation can accurately predict the aerodynamic forces on this missile geometry.

IV. CONCLUDING REMARKS

The following major conclusions can be drawn from this research study.

- A distinctly superior level of agreement was obtained in regards to the axial force coefficient using Missile DATCOM 08, when compared to its predecessor version DATCOM 07. This was made possible by the more detailed geometry that was provided and the predictive ability of Missile DATCOM 8/08 in the transonic and supersonic speed regions.
- Based on a critical comparison between experimental/extrapolated data and Missile DATCOM 8/08, it can be said with relative certainty that Missile axial force predictions can be accomplished with a confidence level of ±10% from the upper transonic to the beginning of the hypersonic speed regions.
- Employing the error correction scheme proposed in Chapter III Section G for the normal force coefficient produces Missile DATCOM output that has a confidence level of ±10% in the range of Mach 1.2 to 3.0 for angles of attack greater than 6º.
- Axial force component level agreements require much finer modeling than is presently available in the semi-empirical models. A far more involved CFD effort may be of some value here.

THIS PAGE INTENTIONALLY LEFT BLANK

V. FUTURE WORK

The continuing development of aerodynamic prediction codes such as Missile DATCOM will drive increased accuracy and promote the increased utility of this aerodynamic prediction tool. As accuracy increases, less time will have to be spent using more expensive (e.g., more time, higher cost) computational tools and performing expensive experiments. The necessity to use these more expensive tools will not be eliminated altogether, however. Essentially, the key to maximizing the benefit for all the more expensive computational tools available is to use programs such as Missile DATCOM, which produce fairly accurate results, to steer analyses that must be performed using these tools.

The goal of this project was to produce an in-house capability to quickly analyze missile designs from this academic institution and the defense industry (through collaborative efforts). The base is now set for using Missile DATCOM as a regular computational tool, whether it be for instructional use, intelligence analyses, or full-scale design.

THIS PAGE INTENTIONALLY LEFT BLANK

APPENDIX A

Appendix A presents the summary derivation of concepts that may be important, but do not necessarily need to remain in the body of this work.

A. VAN DYKE HYBRID THEORY

Van Dyke (1952) postulated that higher-order solutions to the full potential equation could be beneficial if viscous effects were indeed small (Mendenhall & Hemsch, 1992). This theory combines a second-order axial flow solution to the potential equation with a first-order cross flow solution (Moore, 2000). Because perturbations in the flow from the body have more effect in the axial direction, a second-order solution is required to get the desired accuracy particularly for drag calculations. However, perturbations in the cross flow are less sensitive to the body's presence so a first-order approximation provides the necessary accuracy. The cross flow calculations produce the normal and center of pressure distributions. For the body, the nose shape plays a major role in the size of the perturbations produced. If the nose is slender and long, the perturbations will be small and a first-order solution may be employed. However, in reality, this configuration is rarely seen in practice. So in order to achieve the goal of ±10% accuracy a second-order solution must be employed (Moore, 2000).

The following series of equations lay out the general way that VDHT is used to calculate the flow conditions for the supersonic flow field. This summary of the VDHT method is a synthesis of explanations of the method provided by Jenn (Mendenhall & Hemsch, 1992, pp. 44–50) and Moore (2000, pp. 52-57). To begin the second order solution of the full potential equation, all the third order terms are eliminated. However, Van Dyke proposed not eliminating all third order terms, but instead, retaining those that involve only derivatives normal to the freestream. Thus, the perturbation form of the full potential equation becomes

$$\Phi_{rr}+\frac{1}{r}\Phi_r+\frac{1}{r^2}\Phi_{\varphi\varphi}-\beta^2\Phi_{xx}=M_\infty^2\left\{\begin{array}{l}\left[2+(\gamma-1)M_\infty^2\right]\Phi_x\Phi_{xx}+2\Phi_r\Phi_{xr}\\+\frac{2}{r^2}\Phi_\varphi\Phi_{x\varphi}+\Phi_r^2\Phi_{rr}+\frac{2}{r^2}\Phi_r\Phi_\varphi\Phi_{r\varphi}\\-\frac{1}{r^3}\Phi_r^2\Phi_\varphi+\frac{1}{r^4}\Phi_\varphi^2\Phi_{\varphi\varphi}\end{array}\right\} \tag{16}$$

where $\beta=\sqrt{1-M_\infty^2}$. If all the terms that are second-order or greater are neglected in Eq. (16) we can see that it reduces to the first-order perturbation equation.

$$\Phi_{rr}+\frac{1}{r}\Phi_r+\frac{1}{r^2}\Phi_{\varphi\varphi}-\beta^2\Phi_{xx}=0 \tag{17}$$

The two boundary conditions required are as follows:

(a) No disturbances are allowed up stream. This is shown by

$$\Phi_r(0,r,\varphi)=\Phi_x(0,r,\varphi)=0 \tag{18}$$

(b) Flow tangency at the surface of the body given by

$$\Phi_r(x,r_b,\varphi)+\sin\alpha\cos\varphi=\frac{\mathrm{d}r}{\mathrm{d}x}\left[\cos\alpha+\Phi_x(x,r_b,\varphi)\right] \tag{19}$$

The following is proposed as the solution

$$\Phi(x,r,\varphi)=\psi_1(x,r)\cos\alpha+\zeta_1(x,r)\sin\alpha\cos\varphi \tag{20}$$

The first term in Eq. (20) is the first-order axial solution. The second term is the first-order cross flow solution. Van Dyke's theory uses a second order method in the axial direction, but because we need to seed the second-order solution with the first-order solution, we begin with the first-order solution. Additionally, because Eq. (20) is linear, each of these solutions can be found separately and then added together (i.e., principle of superposition). $\psi(x,r)$ is a distribution of sources and sinks along the centerline of the body that satisfies the boundary conditions at all points. $\zeta(x,r)$ is a distribution of doublets along the centerline that satisfies the same boundary conditions as the source distribution.

We now work with each proposed solution separately. First, we tackle the axial flow solution. Differentiating as necessary and substituting $\psi(x,r)$ into Eq. (17), we arrive at

$$\psi_{1rr}+\frac{1}{r}\psi_{1r}-\beta^2\psi_{1xx}=0 \tag{21}$$

Substituting for the boundary conditions, we have

$$\begin{aligned}\psi_{1r}(0,r)&=\psi_{1x}(0,r)=0\\ \psi_{1r}(x,r_b)&=r_b'\left[1+\psi_{1x}(x,r_b)\right]\end{aligned} \tag{22}$$

Second, we tackle the first-order cross flow solution. Differentiating as necessary and substituting $\zeta(x,r)$ into Eq. (17), we arrive at

$$\zeta_{1rr}+\frac{1}{r}\zeta_{1r}-\frac{1}{r^2}\zeta_1-\beta^2\zeta_{1xx}=0 \tag{23}$$

Substituting for the boundary conditions, we have

$$\begin{aligned}\zeta_{1r}(0,r)&=\zeta_{1x}(0,r)=0\\ 1+\zeta_{1r}(x,r_b)&=r_b'\zeta_{1x}(x,r_b)\end{aligned} \tag{24}$$

The general solution for Eq. (21) follows as

$$\psi_1(x,r)=-\int_0^{x-\beta r}\frac{f(\xi)\,\mathrm{d}\xi}{\sqrt{(x-\xi)^2-\beta^2r^2}} \tag{25}$$

The general solution for Eq. (23) follows as

$$\zeta_1(x,r)=\frac{1}{\beta r}\int_0^{x-\beta r}\frac{(x-\xi)\,g(\xi)\,\mathrm{d}\xi}{\sqrt{(x-\xi)^2-\beta^2r^2}} \tag{26}$$

$f(\xi)$ and $g(\xi)$, the source distribution and doublet distribution, respectively, could be linear if only the first-order solution were required. However, they must be of higher order for the second-order solution to be non- trivial.

The next step in the process is the key to the hybrid theory. The first-order solution is used to seed the second-order solution. This is done by creating a second-order axial perturbation equation with the second-order solution on the left and the first-

order axial solution previously determined on the right. We then have the second-order accurate solution in terms of the first-order.

$$\psi_{2rr}+\frac{1}{r}\psi_{2r}-\beta^2\psi_{2xx}=M_\infty^2\left\{\begin{array}{l}2\psi_{1r}\psi_{1xr}+\left[2+(\gamma-1)M_\infty^2\right]\psi_{1x}\psi_{1xx}\\+\psi_{1r}^2\psi_{1rr}+\dfrac{(\gamma-1)}{2}M_\infty^2\psi_{1r}^2\psi_{1xx}\end{array}\right\} \tag{27}$$

The boundary conditions are exactly of the form of Eq. (22), but involve the second order solution. Van Dyke then found a particular solution to Eq. (27). It is given by

$$\left(\psi_P\right)_2=M_\infty^2\left[\psi_{1x}\left(\psi_1+\frac{(\gamma+1)M_\infty^2}{2\beta^2}r\psi_{1r}\right)-\frac{1}{4}r\psi_{1r}^3\right] \tag{28}$$

The formulation of Eq. (28) is the real breakthrough in this theory because the second-order particular solution is given algebraically in terms of the first-order solution. This makes finding the velocity components very simple and involves only differentiating Eq. (28). Now the velocity components are only in terms of the first-order solution.

The full solution to Eq. (27) involves adding a complementary solution and using a boundary condition with both the particular and complementary solutions. We finally use the second-order accurate axial solution and the first-order accurate cross flow solution to formulate the perturbation velocities given by

$$\begin{aligned}\frac{u}{U_\infty}&=\cos\alpha\left(1+\psi_{2x}\right)+\zeta_{1x}\sin\alpha\cos\varphi\\\frac{v}{U_\infty}&=\psi_{2r}\cos\alpha+\sin\alpha\cos\varphi\left(1+\zeta_{1r}\right)\\\frac{w}{U_\infty}&=-\sin\alpha\sin\varphi\left(1+\frac{\zeta_1}{r}\right)\end{aligned} \tag{29}$$

Using the perturbation velocities, we can then find the pressure distribution on the body. It is given by

$$C_p\left(x,\varphi\right)=\frac{2}{\gamma M_\infty^2}\left\{\left[1+\frac{\gamma-1}{2}M_\infty^2\left(1-\frac{u^2+v^2+w^2}{U_\infty^2}\right)\right]^{\frac{\gamma}{\gamma-1}}-1\right\} \tag{30}$$

The drag force coefficient (normal and moment not discussed) is then given by

$$C_A = \frac{2}{\pi r_r^2} \int_0^l \int_0^\pi C_P\left(x,\varphi\right) \frac{r\mathrm{d}r}{\mathrm{d}x} \mathrm{d}\varphi \mathrm{d}x \tag{31}$$

Therefore, we only need use quadratic order source and sink distributions to define the axial and cross flow distributions, perform the integrations numerically, and we get the pressure distribution and the force coefficients from it.

The limitations of the theory are: 1) The range of operation of this theory is from approximately a Mach number of 1.2 to from 2.0 to 3.0, depending on the body configuration; 2) The lower limit corresponds with the condition where weak shocks are present, and the flow field is supersonic with the exception of the boundary layer and areas where the flow may be separated; 3) The upper limit of this theory is governed by the location of the Mach cone with respect to the surface. Thus, it may be used except when Mach cone lies on the surface. The angle of the Mach cone varies with nose angle.

B. TRANSONIC AREA RULE AND VON KÁRMÁN SIMILARITY

The transonic area rule comprises the idea that two bodies with identical cross-sectional areas produce the same wave drag at a particular Mach number. The von Kármán "similarity laws state that, for two-dimensional flow, the flow patterns over two similar, non-lifting airfoils must be the same if the parameter $\left(t/c\right)^{1/3}\left|1-M^2\right|$ has the same value for each airfoil" (Mendenhall & Hemsch, 1992, p. 23). Thus, this can be used to determine unknown values with a range of experimentally determined values.

THIS PAGE LEFT INTENTIONALLY BLANK

APPENDIX B

Tables 5–7 list the axial force coefficient prediction methods employed in Missile DATCOM 8/08 for the body alone, fin alone, and body-fin synthesis.

Parameter	Subsonic/Transonic (M<1.2)	Supersonic (M>1.2)
C_A-skin fricition	Turb: Van Driest II, MDAC West Handbook Lam: Blasius, Hoerner Fluid Dynamics Drag Roughness: USAF Datcom section 4.1.5.1	Turb: Van Driest II, MDAC West Handbook Lam: Blasius, Hoerner Fluid Dynamics Drag Roughness: USAF Datcom section 4.1.5.1
C_A-pressure/ wave	$M<M_{crit}$: USAF Datcom section 4.2.3.1 $M>M_{crit}$: Cubic Polynomial Curve Fit to M=1.2	SOSET, NSWC-TR-81-156 VDHT, NSWC-TR-81-156 Modified Newtonian Theory, NASA-TND-176
C_A-base	Cylinder: NSWC Charts, NSWC-TR-92/509 Boattail: NASA Method, NASA-TR-R-100 Flare: NSWC Charts, NSWC-TR-81-358	Cylinder: NSWC Charts, NSWC-TR-92/509 Boattail: NASA Method, NASA-TR-R-100 Flare: NSWC Charts, NSWC-TR-81-156
C_A-protuberance	M<0.6: Hoerner Fluid Dynamic Drag M>0.6: Cubic curve Fit, AIAA-1994-0027	M<5.0, Modified Newtonian Theory, AIAA-1994-0027 M>5.0, Modified Newtonian Theory
C_A-α	Allen and Perkins Crossflow, NASA TR-1048 AIAA-2009-0907	SOSET, NSWC-TR-81-156 Assumed zero for VDHT and Modified Newtonian Theory AIAA 2005-4833

Table 5. Body Alone Aerodynamic Methodology for Axial Force Coefficient (After Auman, Doyle, Rosema, Underwood, & Blake, 2008, p. 98)

Parameter	Subsonic (M<0.8)	Transonic (0.8<M<1.4)	Supersonic (M>1.4)
C_A-skin fricition	MDAC West Handbook Hoerner Fluid Dynamic Drag USAF Datcom 4.1.5.1	MDAC West Handbook Hoerner Fluid Dynamic Drag USAF Datcom 4.1.5.1	MDAC West Handbook Hoerner Fluid Dynamic Drag USAF Datcom 4.1.5.1
C_A-pressure	Hoerner Fluid Dynamic Drag	Hoerner Fluid Dynamic Drag	Not Applicable
C_A-wave	Not Applicable	M<1.05: zero 1.05<M<1.4: linear fit	Potential Flow Theory, NWL-TR-3018
C_A-bluntness	USAF Datcom 4.1.5.1	USAF Datcom 4.1.5.1	Potential Flow Theory, NWL-TR-3018
C_A-base	Empirical, NWL-TR-2796	Empirical, NWL-TR-2796	Empirical, NWL-TR-2796
C_A-induced	USAF Datcom 4.1.5.2	USAF Datcom 4.1.5.2	Zero

Table 6. Fin Alone Aerodynamic Methodology for Axial Force Coefficient (After Auman, Doyle, Rosema, Underwood, & Blake, 2008, p. 100)

Parameter	Subsonic (M<1.0)	Supersonic (M>1.0)
Body-Fin Upwash, K_w	Empirical correlation, AIAA 96-3395 Folding fin: AIAA 94-0027	Empirical correlation, AIAA 96-3395 Folding fin: AIAA 94-0027
Fin-Body Carryover, K_B	Slender Body Theory, NACA-TR-1307	Slender Body Theory, NACA-TR-1307 AIAA Journal, May 1981 AIAA-2007-3937
Body-Fin Upwash Center of Pressure, xcp_{WB}	Λ>0: USAF Datcom section 4.1.4.2 Λ<0: AFWAL-TR-84-3084	Λ>0: USAF Datcom section 4.1.4.2 Λ<0: AFWAL-TR-84-3084
Body-Fin-Body Carryover Center of Pressure, xcp_{bW}	Lifting Line Theory, NACA-TR-1307 AIAA 94-0027	Slender Body Theory, NACA-TR-1307 AIAA Journal, August 1982
Fin Deflection, Λ_{ij}	Slender Body Theory, AGARD-R-711	Slender Body Theory, AGARD-R-711
Equivalent Angle of Attack	AIAA Journal S&R, July-Aug 1983	AIAA Journal S&R, July-Aug 1983
Body Vortex Strength	Empirical, NWC-TP-5761	Empirical, NWC-TP-5761
Body Vortex Track	Empirical, NWC-TP-5761	Empirical, NWC-TP-5761
Fin Vortex Strength	Line Vortex Theory, NACA-TR-1307	Line Vortex Theory, NACA-TR-1307
Fin Vortex Track	Along Velocity Vector	Along Velocity Vector
Dynamic derivatives	Equivalent Angle of Attack, AIAA 97-2280	Equivalent Angle of Attack, AIAA 97-2280

Table 7. Body-Fin Synthesis Aerodynamic Methodology for Axial Force Coefficient (After Auman, Doyle, Rosema, Underwood, & Blake, 2008, p. 102)

APPENDIX C

Appendix C presents test cases not presented directly in the body, but those the reader may still find as useful information for the output fidelity of Missile DATCOM 8/08.

Panel A

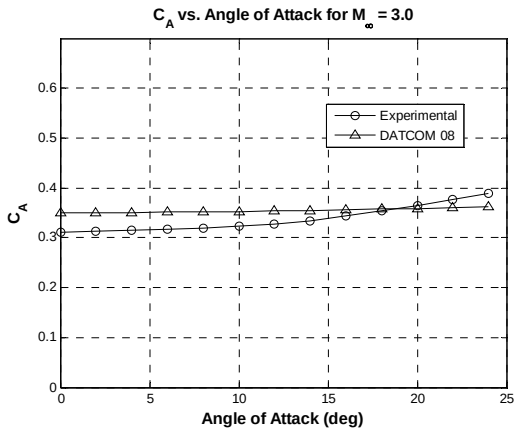

Panel B

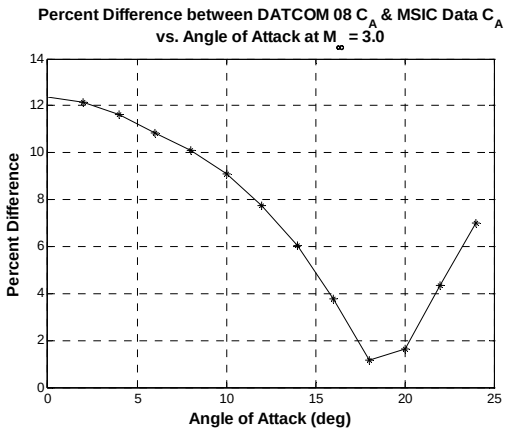

Figure 32. C_A vs. Angle of Attack for MSIC Data and Missile DATCOM 8/08 for M = 3.0 (Panels A and B)

Panel A

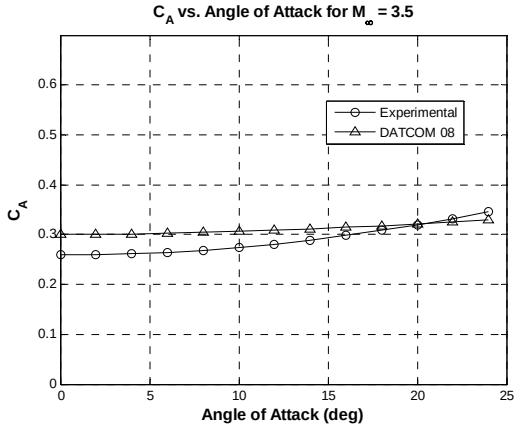

Panel B

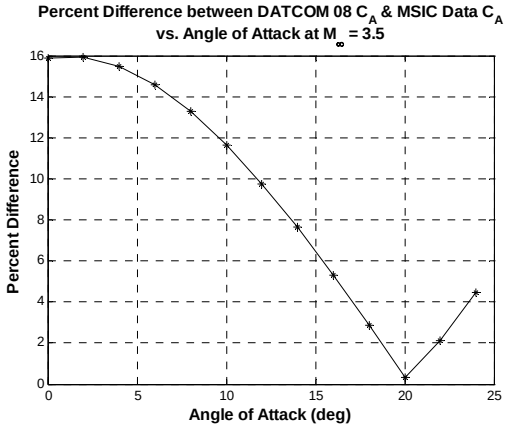

Figure 33. C_A vs. Angle of Attack for MSIC Data and Missile DATCOM 8/08 for M = 3.5 (Panels A and B)

Panel A

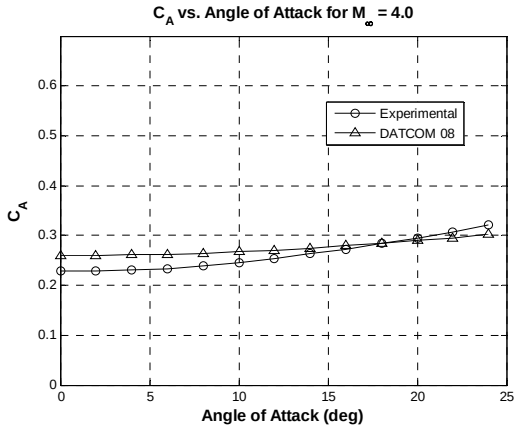

Panel B

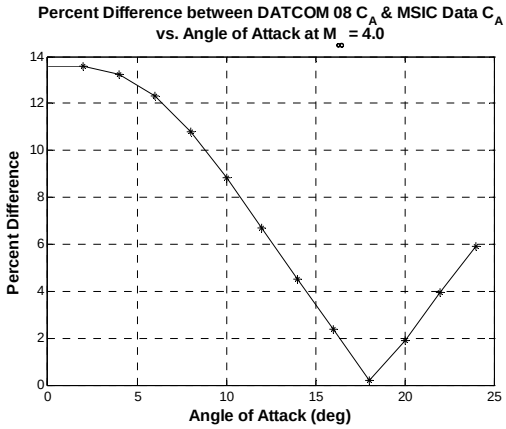

Figure 34. C_A vs. Angle of Attack for MSIC Data and Missile DATCOM 8/08 for M = 4.0 (Panels A and B)

Panel A

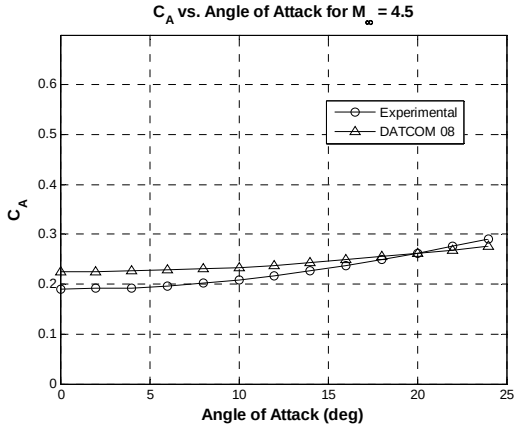

Panel B

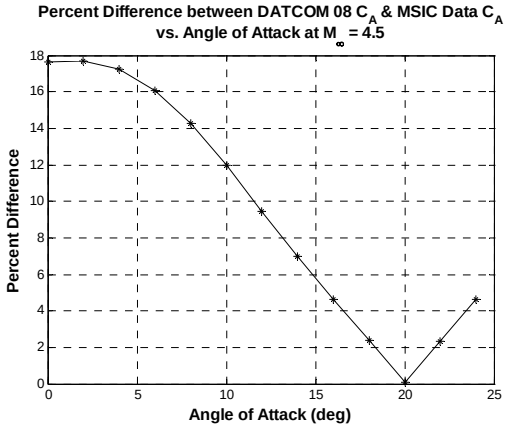

Figure 35. C_A vs. Angle of Attack for MSIC Data and Missile DATCOM 8/08 for M = 4.5 (Panels A and B)

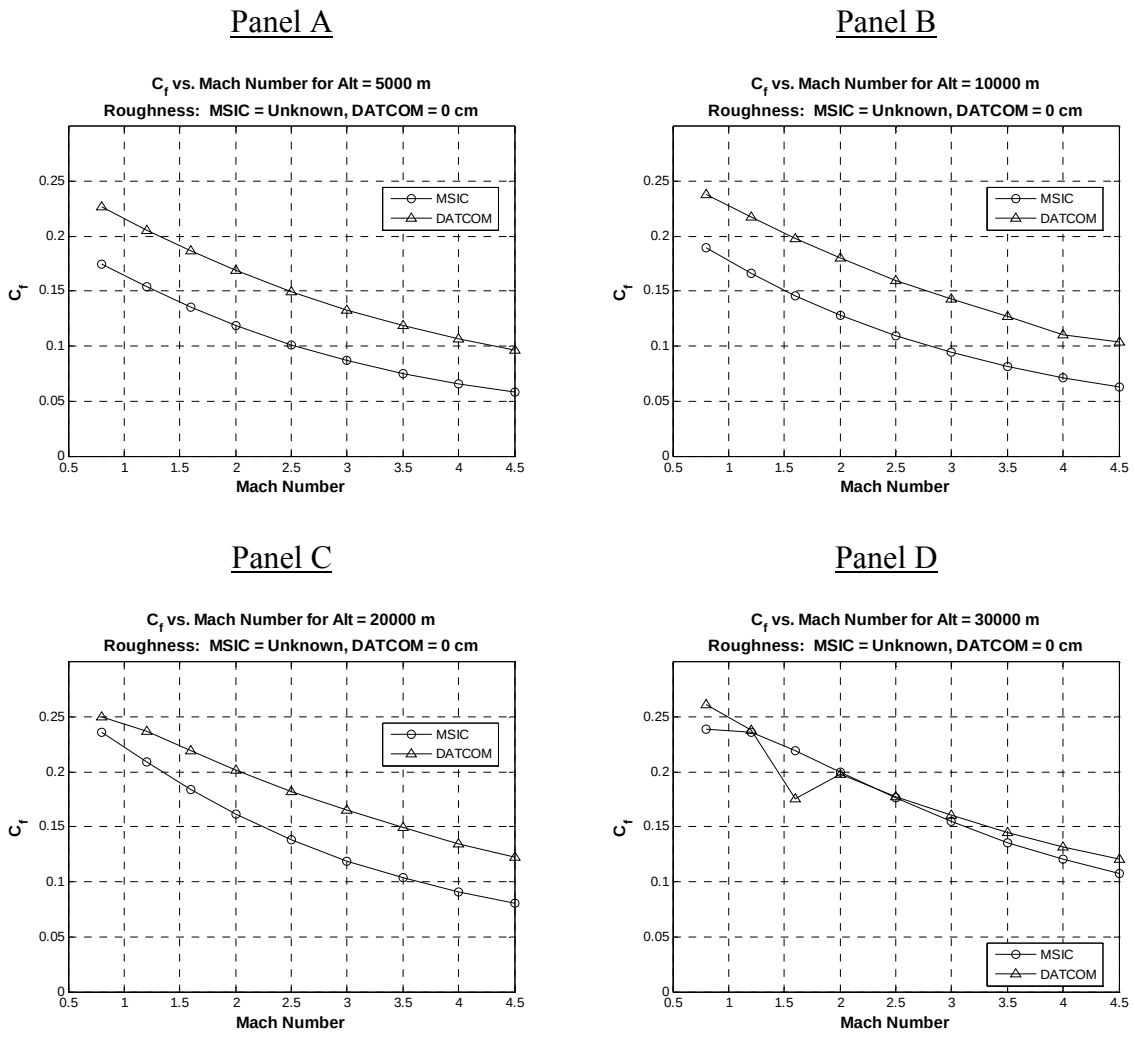

Figure 36. C_f vs. Mach number for MSIC and Missile DATCOM 8/08 at altitudes of 5000 m, 10000 m, 20000 m, and 30000 m (Panels A – D)

Panel A

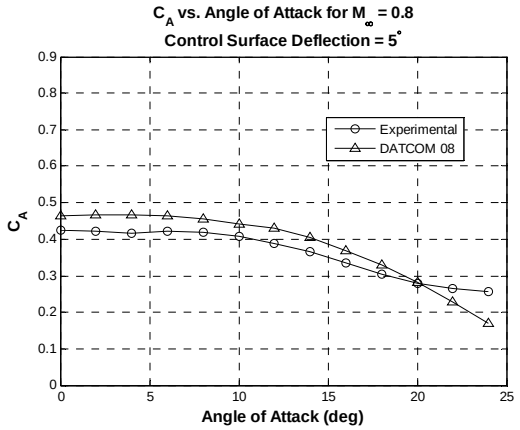

Panel B

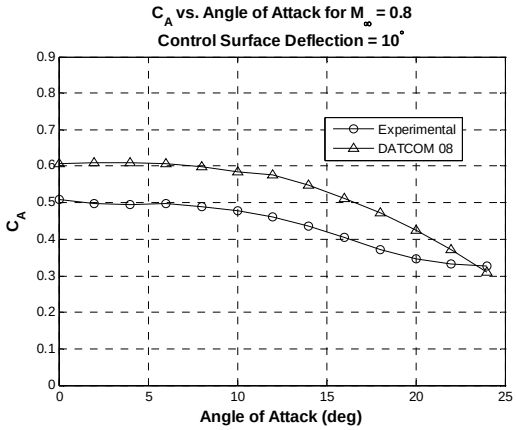

Panel C

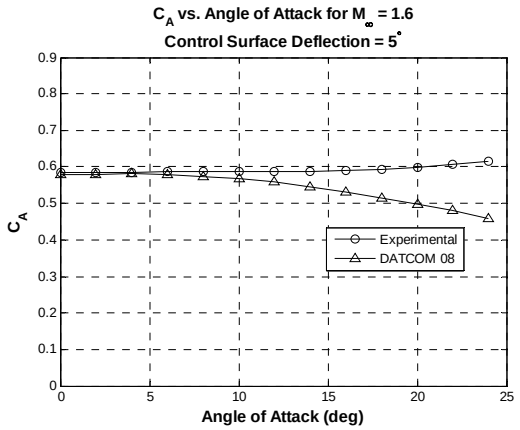

Panel D

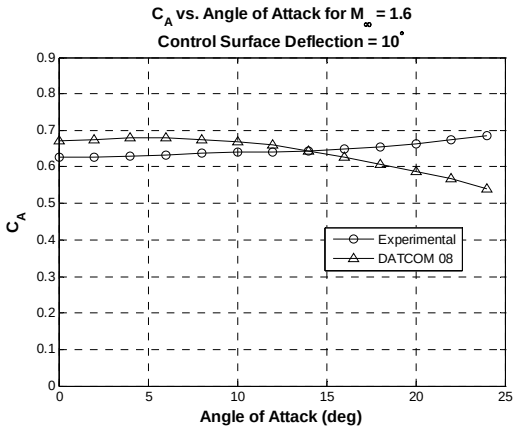

Panel E

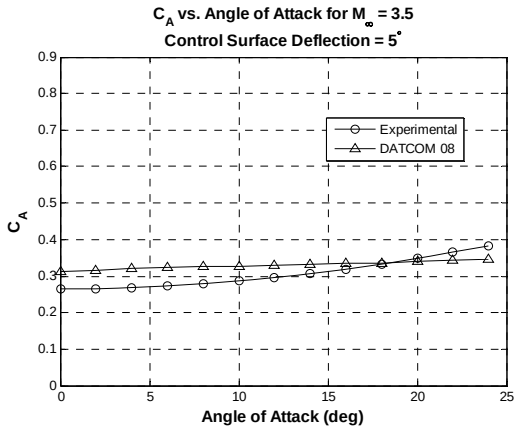

Panel F

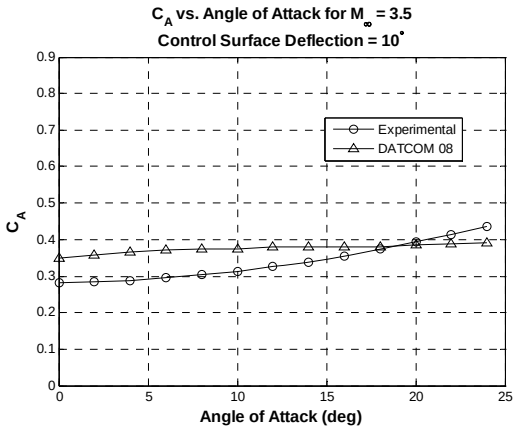

Panel G

Panel H

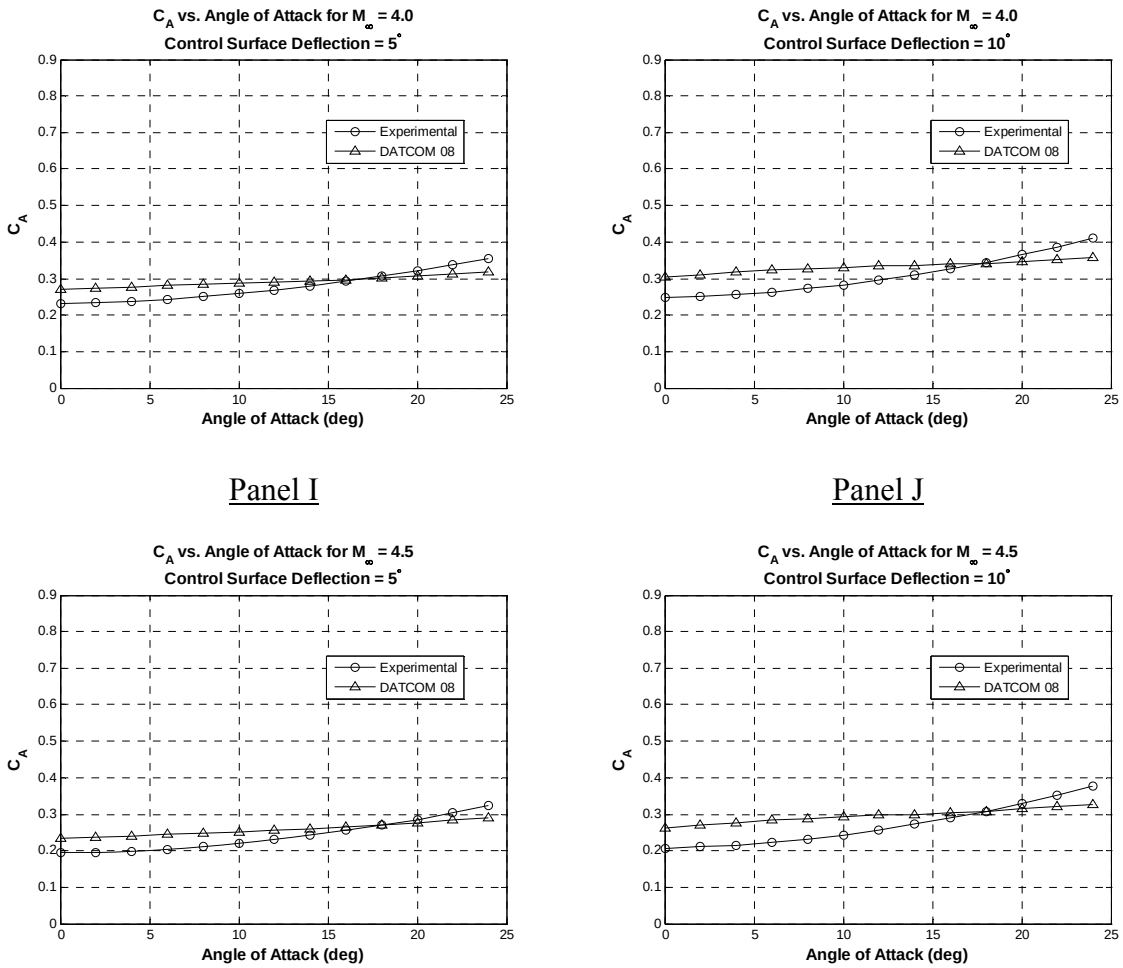

Figure 37. C_A vs. Angle of Attack at M = 0.8, 1.6, 3.5, 4.0, and 4.5 for control surface deflections of 5º and 10º (Panels A – J)

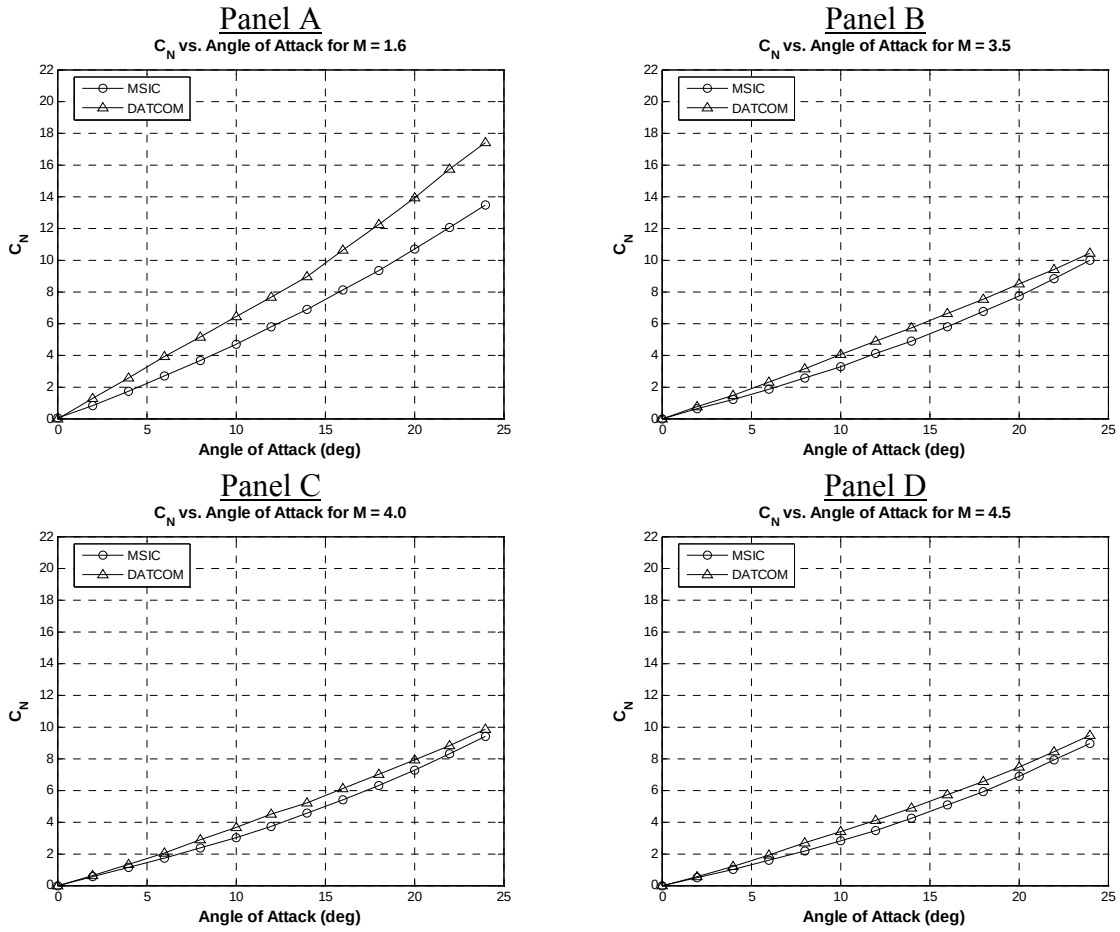

Figure 38. C_N vs Angle of Attack for M = 1.6, 3.5, 4.0, and 4.5 (Panels A-D)

references

LIST OF REFERENCES

Allen, J. H., & Perkins, E. W. (1951). A study of effects of viscosity on flow over slender inclined bodies of revolution No. NACA-TR-1048. Washington, D.C.: National Advisory Council on Aeronautics.

Auman, L., Doyle, J., Rosema, C., Underwood, M., & Blake, W. (2008). MISSILE DATCOM user's manual-2008 revision No. AFRL-RB-WP-TR-2009-3015.

Doyle, J. B., Rosema, C. C., Underwood, M. L., & Auman, L. M. (2009). Recent improvements for the 8/08 release of missile datcom. 47th AIAA Aerospace Sciences Meeting Including the New Horizons Forum and Aerospace Exposition, Orlando, Florida.

Doyle, J. B., Rosema, C. C., Wilks, B. L., & Auman, L. M. (2009). Improvements in finshed vortex treatment for missile datcom. 27th AIAA Applied Aerodynamics Conference, San Antonio, Texas.

Eggers, A. J., Syvertson, C. A., & Kraus, S. (1953). A study of inviscid flow about airfoils at high supersonic speeds No. NACA-TR-1123. Washington, D.C.: National Advisory Council on Aeronautics.

Horton, A. N., & McDaniel, M. A. (2005). Identification and correction of axial force prediction discrepancies due to angle of attack effects in missile DATCOM. 23rd AIAA Applied Aerodynamics Conference, Toronto, Ontario, Canada.

Jorgensen, L. H. (1977). Prediction of static aerodynamic characteristics for slender bodies alone and with lifting surfaces to very high angles of attack No. NASA TR-R-474. Washington, D.C.: National Aeronautics and Space Administration.

Mendenhall, M. R., & Hemsch, M. J. (Eds.). (1992). Tactical missile aerodynamics: Prediction methodology (2nd ed.). Washington, DC: American Institute of Aeronautics and Astronautics.

Moore, F. G. (2000). Approximate methods for weapon aerodynamics American Institute of Aeronautics and Astronautics.

Syvertson, C. A., & Dennis, D. H. (1957). A second-order shock expansion method to inclined bodies of revolution traveling at high supersonic speeds No. NACA-TR-1323. Washington, D.C.: National Advisory Council on Aeronautics.

Teo, H. H. (2008). Aerodynamic predictions, comparisons, and validations using missilelab and missile datcom. Master's thesis, Naval Postgraduate School.

Van Dyke, M. D. (1952). Practical calculation of second-order supersonic flow past nonlifting bodies of revolution No. NACA-TN-2744. Washington, D.C.: National Advisory Committee on Aeronautics.

INITIAL DISTRIBUTION LIST

1. Defense Technical Information Center
   Ft. Belvoir, Virginia

2. Dudley Knox Library
   Naval Postgraduate School
   Monterey, California

3. Professor M. S. Chandrasekhara
   Department of Mechanical and Astronautical Engineering
   NASA Ames Research Center, M.S. 215-1
   Moffett Field, California